1 **Title: Tissue-specific improvements in CD4$^+$ T cell responses after treatment for**
2 **visceral leishmaniasis.**

3 **Authors:** Jessica A. Engel[1], Fabian de Labastida Rivera[1], Benjamin Crawford[1], Hyun
4 Jae Lee[2], Jinrui Na[1], Karshing Chang[1], Kate H. Gartlan[1], Luzia Bukali[1], Teija C.M
5 Frame[1], Yulin Wang[1], Ashraful Haque[2], Christian R. Engwerda[1*]

6 [1]QIMR Berghofer Medical Research Institute, Brisbane, QLD 4006, Australia

7 [2]Department of Microbiology and Immunology, University of Melbourne, located at the
8 Peter Doherty Institute for Infection and Immunity, Parkville, VIC 3000, Australia

9 ***Correspondence**: Christian.Engwerda@qimr.edu.au, Phone: +61 733620428

10 **Conflict of interest statement**: The authors have declared that no conflict of interest
11 exists.

## Abstract

Visceral leishmaniasis (VL) is a life-threatening parasitic disease that requires robust $CD4^+$ T cell-mediated immunity for parasite control. However, the heterogeneity and transcriptional dynamics of $CD4^+$ T cell responses in VL remain poorly defined. In this study, we use a model of experimental VL with tissue-specific immunity and single-cell RNA sequencing to provide a high-resolution assessment of $CD4^+$ T cell responses. Our analysis reveals the complexity of $CD4^+$ T cell differentiation in VL, identifying distinct Th1 subsets with transcriptional heterogeneity that may reflect functional specialisation. Despite minimal transcriptional differences between splenic and hepatic $CD4^+$ T cells, we identified shifts in subset composition, including the emergence of a stem-like $CD4^+$ T cell population in the spleen, which was suppressed by the transcription factor Bhlhe40. *Bhlhe40* deficiency skewed $CD4^+$ T cell differentiation, impairing Th1 responses while promoting Tr1 cells, resulting in defective parasite control in the liver. Additionally, AmBisome treatment induced a profound transcriptional shift in $CD4^+$ T cells, leading to the maintenance of stem-like $CD4^+$ T cells in the spleen and the expansion of tissue resident memory-like cells in the liver. These findings uncover key regulatory mechanisms that shape $CD4^+$ T cell differentiation in VL and provide insights into how immune-modulatory strategies could enhance long-term immunity.

## Introduction

Visceral leishmaniasis (VL) is a potentially fatal parasitic disease caused by the protozoan parasites *Leishmania donovani* and *L. infantum*. These parasites are transmitted to humans through the bite of infected female sand flies and ultimately infect tissue-resident macrophages in internal organs such as the spleen and liver. VL is endemic in countries in South Asia, East Africa, and South America, and is estimated to cause around 50,000 deaths annually[1]. Despite the availability of effective drugs, VL remains a significant health problem in many parts of the world, particularly in resource-limited settings[2,3,4,5]. There is a need for improved diagnostic tools and more effective treatments, as well as efforts to prevent the spread of the disease through vector control and other measures. However, sustained VL elimination will need an effective vaccine that promotes the development of durable and tissue-specific, anti-parasitic $CD4^+$ T cells to prevent outbreaks, especially as case numbers decline and natural immunity wanes as a result of vector control and case-detection measures.

Findings from pre-clinical VL models have shown that following infection, dendritic cells (DCs) capture and present parasite antigens to naïve $CD4^+$ T cells in secondary lymphoid tissues, including the spleen[6]. Pattern recognition receptors expressed by DCs are activated by parasite products and trigger IL-12 production that promotes development of pro-inflammatory $Tbet^+$ $IFN\gamma^+$ $CD4^+$ T helper 1 (Th1) cells[7,8,9]. There is considerable heterogeneity in the molecules Th1 cells express that arises from tissue-specific adaptions for infection control and disease prevention[10]. Regardless, the pro-inflammatory cytokines produced by these Th1 cells are critical for activating phagocytes to kill captured or resident parasites.

The inflammatory products produced by Th1 cells may also damage tissues, and as such, Th1 cells need to be tightly regulated. An important way this occurs is by autologous IL-10 production that inhibits T cell functions and upstream activities of antigen presenting cells (APCs)[11]. IL-10-producing Th1 (type I regulatory T (Tr1)) cell subsets are distinct from Foxp3-expressing regulatory T (Treg) cells that are important for maintaining tissue homeostasis, and comprise a significant proportion of antigen-specific $CD4^+$ T cells in VL patients[12]. However, Tr1 cells not only protect tissues, but they may also allow persistent

60 infection by suppressing immune responses via production of anti-inflammatory
61 cytokines, as well as expression of co-inhibitory receptors[13,14,15,16]. Furthermore, they may
62 also restrict responses to vaccination and the effective generation of anti-parasitic
63 immunity[7,15]. Thus, the balance between parasite-specific Th1 and Tr1 cells in infected
64 tissues is an important determinant of disease outcomes.

65 Given the spleen and liver are important sites of infection and disease in VL patients,
66 much of our knowledge about tissue-specific $CD4^+$ T cell differentiation dynamics has
67 come from a pre-clinical model of VL caused by infection of C57BL/6 mice with the human
68 pathogen *L. donovani*[17,18,19]. In this model, the liver is a site of acute, resolving infection
69 with highly effective anti-parasitic $CD4^+$ T cells (a balanced Th1 and Tr1 cell response),
70 while the spleen is a site of chronic infection and ineffective $CD4^+$ T cells (unbalanced
71 and/or dysregulated Th1 and Tr1 cell response). Thus, the liver responds to infection like
72 infected, asymptomatic individuals (around 90% of *L. donovani*-infected individuals in the
73 Indian sub-continent[3]), while the spleen has a similar disease outcome to that observed
74 in VL patients. The reason for the development of these organ-specific, anti-parasitic
75 $CD4^+$ T cell responses is unknown.

76 In this study, we investigated tissue-specific $CD4^+$ T cell responses in C57BL/6 mice
77 following *L. donovani* infection to delineate how $CD4^+$ T cell transcriptional landscapes
78 vary across different tissues in acute versus chronic inflammatory environments. By
79 comparing immune responses in distinct tissue sites, we aimed to identify key differences
80 in $CD4^+$ T cell dynamics that contribute to protective immunity or immune dysfunction
81 during infection. Additionally, we examined drug-mediated $CD4^+$ T cell responses by
82 assessing the impact of anti-parasitic treatment with AmBisome, a liposomal formulation
83 of amphotericin B, which has been linked to the induction of long-lasting immunity in VL
84 patients. This protection is thought to be driven by the maintenance of antigen-
85 experienced $CD4^+$ T cells capable of sustaining anti-parasitic immunity[19]. However, how
86 AmBisome treatment influences the preservation or reshaping of $CD4^+$ T cell populations,
87 particularly in the context of chronic infection, remains unclear. By distinguishing between
88 tissue-specific and treatment-induced changes in $CD4^+$ T cell responses, we aimed to
89 elucidate the mechanisms underpinning durable immunity following infection and

90 therapeutic intervention. Our findings enabled the construction of a high-resolution
91 transcriptomic atlas of $CD4^+$ T cell responses in experimental VL, capturing the gene
92 expression landscapes across diverse tissue microenvironments. We identified distinct
93 transcriptional programs that define $CD4^+$ T cell subsets in acute and chronic infection,
94 as well as those shaped by anti-parasitic drug treatment. This analysis uncovered
95 molecular signatures distinguishing effector, regulatory, and stem-like $CD4^+$ T cell
96 populations, providing a framework for understanding their functional roles. Additionally,
97 we characterised the dynamic transitions in $CD4^+$ T cell states during infection resolution,
98 offering deeper insights into the regulatory mechanisms that govern $CD4^+$ T cell-mediated
99 immunity in VL.

100 **Results**

101 **Single cell RNA sequencing reveals a heterogeneous Th1 cell response during**
102 **experimental VL.**

103 To understand how $CD4^+$ T cell responses are shaped by acute versus chronic
104 inflammatory environments, we performed transcriptomic profiling of genetically modified
105 T cell receptor transgenic (PEPCK) $CD4^+$ T cells in experimental VL[20]. PEPCK is a
106 naturally processed immunodominant antigen derived from *Leishmania* glycosomal
107 phosphoenol-pyruvate carboxykinase ($PEPCK_{335-351}$) conserved in all pathogenic
108 *Leishmania* species[21]. We transferred $10^4$ naïve PEPCK cells from CD45.2 C57BL/6 mice
109 to CD45.1 C57BL/6 mice and infected one day later with *L. donovani*. Using the CD45.2
110 congenic marker, we isolated transferred PEPCK cells and captured single cell
111 transcriptomes of PEPCK cells from the spleen and liver on day 0, 14, 21,28 and 56 post-
112 infection (p.i.) and performed droplet-based single cell RNA sequencing (scRNAseq)
113 (Figure 1a; Extended Data Figure 1a). In addition, to examine how drug treatment
114 modulates $CD4^+$ T cell responses (required for drug-mediated, life-long protection against
115 reinfection[22], we treated a group of mice with AmBisome, the current recommended VL
116 therapy for patients in India[4]), or vehicle control. In comparison to vehicle control-treated
117 mice, AmBisome treatment led to significant reductions in organ weight and total cell
118 numbers (Extended Data Figure 1b and c), indicating effective parasite clearance and
119 resolution of infection-associated inflammation.

120 To control for batch effects between time points, naïve PEPCK transcriptomes were
121 captured at each time point. Principle component analysis (PCA) revealed that naïve
122 PEPCK transcriptomes from each time point overlapped indicating no batch effects from
123 time point were present in the dataset (Extended Data Figure 2a). After performing quality
124 control checks for naïve and activated genes (*Sell, Ccr7, Cd44, Tbx21*) and due to the
125 transcriptomic distance of naïve PEPCK from all other time points (Extended Data Figure
126 2b and c), naïve PEPCK were removed from downstream analysis. In addition, to focus
127 on transcriptomic heterogeneity, T cell receptor alpha and T cell receptor beta genes were
128 removed from the dataset prior to further analysis and clustering.

129 After quality control, 40,667 cells were taken forward for analysis. UMAP visualisation
130 revealed substantial overlap in $CD4^+$ T cell transcriptomes between acute (liver) and
131 chronic (spleen) inflammatory environments (Figure 1b), suggesting shared
132 transcriptional programs across tissues. Unsupervised clustering defined 16 clusters
133 (Figure 1c; Extended Data Figure 2d & e), which included 3 main clusters (>10% of total
134 cells; Clusters 1-3), 6 intermediate clusters (3-10% of total cells; Clusters 4-9) and 7 minor
135 clusters (<3% of total cells; Clusters 10-16). All clusters were observed by day 14 p.i. with
136 little evidence of progressive change after day 21 p.i. over the course of infection (Figure
137 1d), indicating that patterns in $CD4^+$ T cell responses are established early during
138 infection and do not undergo significant diversification as the infection progresses. Cell
139 clusters were annotated using cluster marker genes (Figure 1e) and included; effector
140 cells expressing *Cxcr3, Jun* and *Fos* (Cluster 2), and *Klrg1*, *Zeb2*, *S1pr5*, *Ifng* (Cluster 3),
141 and *Ccl3*, *Ccl4* and *Gzmb* (Cluster 8), and *Gzma* (Cluster 10); Tr1-like cells (Cluster 1)
142 expressing *Lag3*, *Tigit*, *Pdcd1* and *Il10*; memory-like cells expressing *Cd7*, *Il7r, Cxcr6*
143 (Cluster 5) and *Tcf7, Ccr7* (Cluster 7); cells expressing heat shock stress pathway genes
144 (Cluster 6) and type I interferon stimulated genes (Cluster 15); proliferative cells (Cluster
145 12, 13, 14) expressing cell cycle genes (Figure 1f). In addition, PEPCK cells in the
146 proliferative clusters, as well as in Cluster 1, showed increased aerobic glycolysis activity
147 (Figure 1f). Assessment of the expression of lineage marking transcription factors showed
148 that PEPCK cells in all clusters, but not naïve PEPCK (Extended Data Figure 2c),
149 expressed high levels of *Tbx21* and upregulated genes associated with a Th1 cell gene
150 signature (Figure 1g), consistent with a Th1 cell phenotype, as previously reported in

151 experimental VL[16]. These data suggest that during experimental VL, CD4⁺ T cells
152 diversify into various Th1 cell subtypes with distinct gene expression profiles.

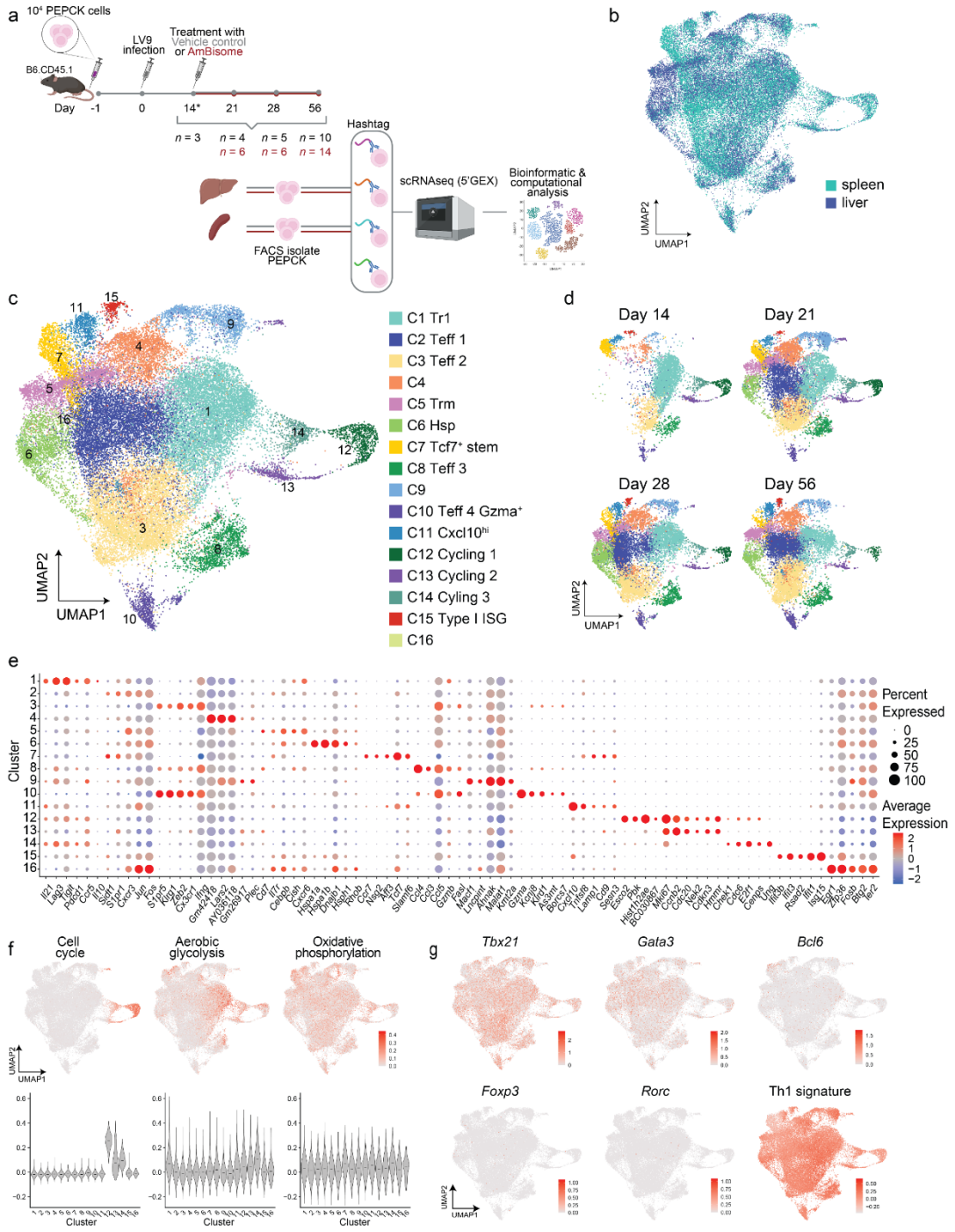


***Figure 1. scRNAseq reveals a heterogeneous Th1 cell response during experimental visceral leishmaniasis. (a)*** *$10^4$ PEPCK cells (CD45.2⁺) were adoptively transferred to B6.CD45.1⁺ mice, which were then infected with L. donovani the next day. PEPCK cells were isolated from the spleen and liver at various time points post-infection and subjected to*

*scRNAseq.* ***(b)*** *UMAP visualisation of 40,667 PEPCK from day 14 – 56 p.i. in experimental VL showing tissue, and* ***(c)*** *unsupervised clustering analysis.* ***(d)*** *UMAP visualisation showing clusters subsetted by time point p.i.. Colours correspond to clusters in (c).* ***(e)*** *Dot plot showing the average expression of curated marker genes for each cluster.* ***(f)*** *Cell cycle, aerobic glycoloysis and oxidative phosphorylation gene signature scores visualised on UMAP and quantified in violin plots. Median line shown on violin plots.* ***(g)*** *UMAP visualisations showing the expression of T helper cell lineage-defining transcription factors and a Th1 cell gene signature.*

153 **Transcriptional similarity of CD4$^+$ T cells in distinct tissues and reprogramming**
154 **following AmBisome treatment during experimental VL.**

155 To investigate the influence of tissue environment and drug treatment on CD4$^+$ T cell
156 differentiation, we examined the distribution of PEPCK cells across clusters. Although
157 PEPCK cells were detected across all clusters in most samples, their relative proportions
158 varied depending on time point, tissue, and treatment (Figure 2a & b; Extended Data
159 Figure 3). Overall, the transcriptional profiles of CD4$^+$ T cells in the spleen and liver from
160 control-treated mice were similar, with most clusters following similar temporal dynamics
161 across both organs. Notable organ-specific differences in cluster frequencies included
162 Cluster 6, associated with heat shock stress pathways, which was more prevalent in the
163 liver at day 21 p.i.. Additionally, Cluster 7, comprising *Tcf7*-expressing PEPCK cells,
164 peaked in frequency at day 14 p.i. and was largely spleen-specific. Taken together, these
165 data suggest that CD4$^+$ T cells in the spleen and liver exhibit largely comparable
166 transcriptional programs throughout infection, indicating that factors beyond T cell intrinsic
167 transcriptional differences, such as the tissue microenvironment, likely drive organ-
168 specific infection outcomes.

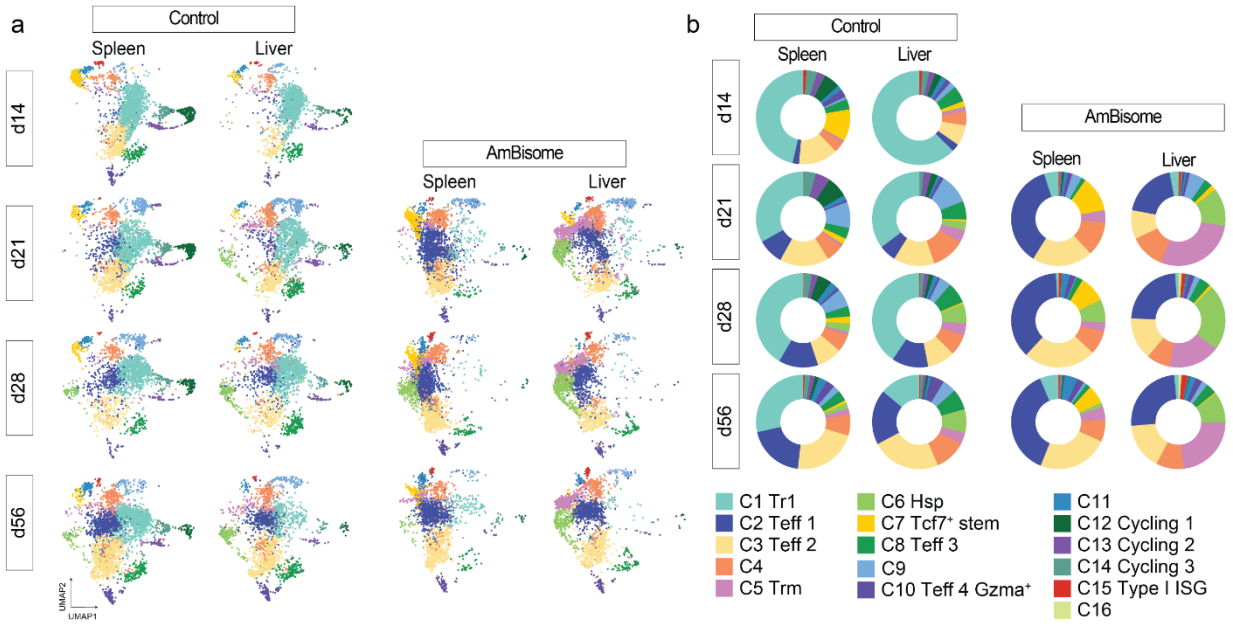


***Figure 2. Tissue-specific CD4⁺ T cell responses in experimental VL. (a)*** *UMAP visualisation showing PEPCK cells at day 14-56 p.i. in experimental VL subsetted by time point, organ and treatment.* ***(b)*** *Donut plots show the proportion of PEPCK cells from each sample per cluster. Colours correspond to clusters in (a).*

169 We next investigated the impact of AmBisome treatment on CD4⁺ T cell transcriptional
170 profiles and their developmental trajectories. Strikingly, AmBisome treatment induced
171 substantial shifts in cluster frequencies, suggesting a pronounced impact on CD4⁺ T cell
172 dynamics. Most notably, the proportion of Tr1 cell PEPCK cells (Cluster 1) was
173 dramatically reduced following treatment, while effector PEPCK cell populations (Clusters
174 2 and 3) expanded in both the spleen and liver. Additionally, Cluster 7, a *Tcf7*⁺ spleen-
175 associated population, was maintained at a higher frequency beyond day 14 p.i. in
176 AmBisome-treated mice, instaed of declining like in untreated controls. In the liver, Cluster
177 5, which exhibited tissue resident memory (Trm)-like characteristics, expanded
178 significantly following drug treatment. Overall, while some tissue-specific differences were
179 observed in untreated mice, the most striking changes were driven by drug treatment.
180 AmBisome not only sustained the presence of splenic *Tcf7*-expressing cells throughout
181 infection but also promoted the development of Trm-like PEPCK cells in the liver,
182 highlighting its capacity to shape distinct CD4⁺ T cell subsets across tissues.

183 These transcriptomic findings were validated at the protein level through flow cytometry
184 analysis of PEPCK cells isolated from the spleen and liver of *L. donovani* infected mice
185 at days 14, 28, and 56 p.i., including a cohort treated with AmBisome at day 14 p.i.
186 (Extended Data Figure 4a and b). Flow cytometry revealed substantial heterogeneity in
187 surface marker expression among PEPCK cells, mirroring the diversity observed in
188 transcriptional profiling (Extended Data Figure 4c and d). All PEPCK cells expressed Tbet
189 and CD44, confirming an activated Th1 phenotype. TCF1 expression was observed to be
190 the highest in the spleen at day 14 p.i., and was sustained at later time points following
191 AmBisome treatment, compared to in control-treated mice. AmBisome treatment also
192 resulted in reduced PD1 expression in both the spleen and liver, suggesting a potential
193 alleviation of T cell exhaustion. Additionally, AmBisome treatment led to upregulation of
194 CXCR6 and CD69 expression in the liver, consistent with an expansion of tissue-resident
195 cells, while CD127 expression increased in both the spleen and liver, indicative of
196 enhanced survival potential.

197 To further define these populations, unsupervised clustering of PEPCK cell FACS data
198 identified 18 distinct clusters (Extended Data Figure 4e and f). These included seven
199 effector clusters, two memory-like clusters (tissue-resident memory [Trm] and central
200 memory [Tcm]), and nine TCF1$^{+}$ clusters distinguished by differential expression of
201 CCR7, CD127, CXCR6, PD1, and KLRG1. Consistent with transcriptional data, the
202 frequency of these clusters varied by tissue, time point, and treatment (Extended Data
203 Figure 4g). Overall, these findings confirm the heterogeneity of Th1 cells at the protein
204 level and demonstrate that tissue environment and drug treatment drive distinct Th1
205 subset frequencies within the CD4$^{+}$ T cell response during experimental VL.

206 **Polyclonal CD4$^{+}$ T cell responses resemble PEPCK cell responses at the**
207 **transcriptomic level.**

208 The diversity of the T cell receptor (TCR) repertoire has been shown to influence CD4$^{+}$ T
209 cell responses by affecting clonal selection, signal strength, and subsequent
210 differentiation into distinct effector and memory subsets[23,24]. In experimental VL, we
211 observed diversity within Th1 cells, but limited transcriptomic differences between CD4$^{+}$
212 T cells from the spleen and liver. To determine whether these patterns are influenced by

213 lack of T cell receptor (TCR) diversity, we investigated whether T cell clonality drives
214 effector fate choices or tissue localisation, and whether the lack of transcriptomic variation
215 reflects a limited repertoire of TCR diversity. We used scRNAseq to compare the
216 transcriptomes of PEPCK cells (monoclonal) and polyclonal *Leishmania*-specific $CD4^+$ T
217 cells during experimental VL. Congenic wild-type mice were infected with *L. donovani* and
218 polyclonal *Leishmania*-specific $CD4^+$ T cells were isolated at day 14 p.i. from the spleen
219 and liver by staining with a *Leishmania*-specific MHC-class II I-$A^b$ tetramer (I-$A^b$
220 $PEPCK_{335-351}$)[25,26], and cells were then sorted. This time point is the peak of acute
221 infection in the liver and marks the establishment of infection in the spleen in experimental
222 VL[19]. To minimise non-specific binding to the I-$A^b$ $PEPCK_{335-351}$ tetramer, we co-stained
223 with a negative control MHC-class II I-$A^b$ tetramer loaded with a non-specific human CLIP
224 peptide (I-$A^b$ $CLIP_{87-101}$) (Extended Data Figure 5a). Activation of isolated I-$A^b$ $PEPCK_{335-}$
225 $_{351}{}^+$ cells was confirmed by co-expression of CD49b and CD11a (Extended Data Figure
226 5b) and the transcriptomes were then assessed using droplet-based scRNAseq coupled
227 with TCR V(D)J sequencing using the 10x Chromium platform. Due to constraints in
228 isolating sufficient numbers of cells, cells from multiple mice were pooled for scRNAseq
229 as described in the methods. This resulted in single cell transcriptomic data for 5,348 I-
230 $A^b$ $PEPCK_{335-351}{}^+$ cells (2,935 cells from the spleen and 2,413 cells from the liver) after
231 excluding poor quality single cell transcriptomes (Extended Data Figure 5c), which were
232 then merged with scRNAseq data from splenic and hepatic PEPCK cells at day 14 p.i
233 (from Figure 1).

234 PEPCK and I-$A^b$ $PEPCK_{335-351}{}^+$ cells from the spleen and liver showed significant
235 transcriptomic overlap when visualised by UMAP (Figure 3a). Clustering of PEPCK and
236 I-$A^b$ $PEPCK_{335-351}{}^+$ cells at day 14 p.i. defined 17 clusters (Figure 3b), including 4 main
237 clusters (Clusters 1-4), 6 intermediate clusters (Clusters 5-10) and 7 minor clusters
238 (Clusters 11-17). As defined using cluster marker genes, similar $CD4^+$ T cell subsets were
239 identified as before for the PEPCK cell longitudinal data. This included Tr1 cells (Cluster
240 2) expressing high levels of *Lag3* and *Il10*; effector cells (Clusters 1, 4, 7, 15) expressing
241 effector genes *S100a4*, *Ccl5*, *Nkg7*, *Gzma*; proliferative cells (Clusters 6, 9, 12); memory
242 cells expressing high levels of *Tcf7* and *Ccr7* (Cluster 4). PEPCK and I-$A^b$ $PEPCK_{335-351}{}^+$
243 cells from the spleen and liver were broadly distributed across all clusters, excluding

244 Clusters 13, 15, and 17 (Figure 3c). Clusters 13 and 17 were predominantly composed
245 of I-$A^b$ $PEPCK_{335-351}^+$ cells, with Cluster 13 enriched for cells expressing heat shock stress
246 pathway genes and Cluster 17 representing a minor population of only 36 cells. A similar
247 heat shock stress-associated cluster was also identified in the longitudinal PEPCK cell
248 dataset (Figure 1; Cluster 6), but it was only identified from day 21 onwards, suggesting
249 that differences in infection kinetics may contribute to this variation and that this signature
250 is not specific to I-$A^b$ $PEPCK_{335-351}^+$ cells. In contrast, Cluster 15 was predominantly
251 composed of PEPCK cells, suggesting that clonotype may influence the likelihood of
252 $CD4^+$ T cells differentiating into *Gzma* expressing effector cells. However, further
253 experimentation is required to confirm this.

254 We next subsetted I-$A^b$ $PEPCK_{335-351}^+$ cells and examined the expression of lineage
255 defining transcription factors. Consistent to the PEPCK cell phenotype during
256 experimental VL, we observed high levels of *Tbx21* and Th1 cell gene signatures in I-$A^b$
257 $PEPCK_{335-351}^+$ cells (Figure 3d). These data indicate that in experimental VL, the
258 transcriptional landscape of TCR-restricted and polyclonal *Leishmania*-specific $CD4^+$ T
259 cells is conserved and closely aligns with Th1 cells.

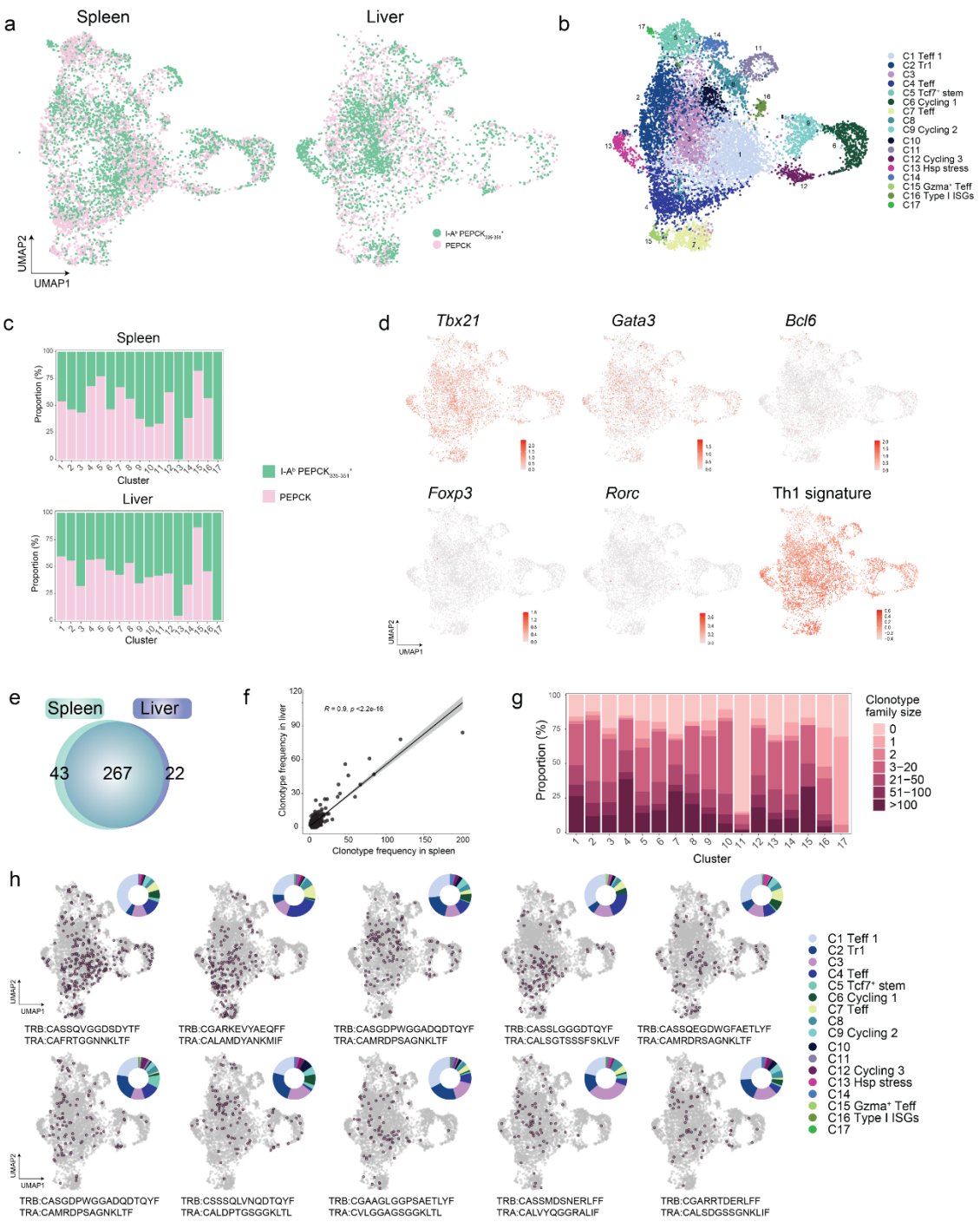


***Figure 3. Leishmania-specific CD4$^+$ T cell differentiation is independent of clonality or tissue localisation in experimental VL.*** ***(a)*** *Droplet-based scRNAseq analysis of 10,696 PEPCK cells and I-A$^b$ PEPCK$_{335-351}$$^+$ cells at day 14 p.i. in experimental VL. UMAP visualisation showing PEPCK and I-A$^b$ PEPCK$_{335-351}$$^+$ cell type, subsetted by organ and* ***(b)*** *the clusters identified.* ***(c)*** *Bar graph shows the distribution of PEPCK cells and I-A$^b$ PEPCK$_{335-351}$$^+$ cells from each organ across clusters.* ***(d)*** *UMAP visualisation showing subsetted I-A$^b$ PEPCK$_{335-351}$$^+$ cells and the expression of master T helper cell transcription factors.* ***(e)*** *Venn diagram shows the distribution*

*of 332 clonotypes identified with two or more family members in the I-A$^b$ PEPCK$_{335-351}^+$ cells at day 14 p.i. between the spleen and liver.* ***(f)*** *Pearson's correlation of the frequency of I-A$^b$ PEPCK$_{335-351}^+$ cell clonotypes, with two or more family members, in the spleen and liver.* ***(g)*** *Bargraph showing the distribution of all I-A$^b$ PEPCK$_{335-351}^+$ cell clonotypes in each cluster, grouped by family size.* ***(h)*** *The distribution of the top 10 most frequent I-A$^b$ PEPCK$_{335-351}^+$ cell clonotypes across the UMAP visualisation for I-A$^b$ PEPCK$_{335-351}^+$ cells only. Members of each clonotype are highlighted in pink. The doughnut plot shows the distribution of clonotype across clusters, colours correspond to clusters in (b).*

**Tissue seeding and CD4$^+$ T cell differentiation is largely independent of TCR diversity.**

Next, we investigated how CD4$^+$ T cell clones are seeded between the spleen and liver to determine whether TCR diversity influences CD4$^+$ T cell differentiation in experimental VL. In the I-A$^b$ PEPCK$_{335-351}^+$ cells, we identified a TCR α– and β-chain for 4244 cells (79.36%) of 5348 cells total. Among these cells, we detected 583 clonotype families, defined by the sharing of identical TCR α– and β–chains, with 332 clonotypes that had a family size ≥ 2 cells. However, since the cells were pooled from multiple mice, it is important to note that clonotype diversity at the level of individual mice could not be assessed. To determine how CD4$^+$ T cell clonotype influenced tissue distribution, we compared the localisation of the 332 clonotypes that had expanded. The majority of these clonotypes (80%) were found in PEPCK$_{335-351}^+$ cells isolated from both the spleen and liver, whereas only 43 and 22 clonotypes were unique to the spleen and liver, respectively (Figure 3e). We then compared the frequency of these 332 clonotypes in each tissue. Pearson correlation analysis identified a strong positive correlation indicating that in experimental VL, seeding of CD4$^+$ T cell clonotypes in the spleen and liver occurs at a similar frequency (Figure 3f). To determine whether clonotype influences CD4$^+$ T cell fate choices, we next examined how clonotypes were distributed between clusters. Although varying in frequency, clonotype family expansion was distributed across all clusters (Figure 3g), excluding Clusters 11 and 17 and no preference for a specific cluster was identified for the top 10 most expanded clonotypes (Figure 3h). Overall, these data indicate that TCR diversity had limited impact on CD4$^+$ T cell tissue seeding or cluster differentiation in experimental VL.

283 **AmBisome treatment promotes hepatic tissue-resident memory-like CD4$^+$ T cell**
284 **development.**

285 The clustering analysis in Figure 2 identified Cluster 5 as a transcriptionally distinct,
286 predominantly liver-resident subset that expanded following AmBisome treatment. These
287 characteristics suggest a potential role for this CD4$^+$ T cell subset in localised immune
288 responses during experimental VL. To gain deeper insights into this subset, we performed
289 a detailed analysis of its gene signatures and evaluated its functional relevance in the
290 context of experimental VL.

291 Assessment of Cluster 5 marker genes (Figure 4a) led us to hypothesise that these cells
292 were tissue-resident CD4$^+$ T cells. We detected expression of *Zfp683*, *Cxcr6*, *Itga1*, *Cd69*
293 and *Il7r* (Figure 4b), all of which have previously been linked to tissue-resident memory
294 cells[27,28]. In addition, Cluster 5 was enriched for a CD8$^+$ T cell Trm-gene signature[28]
295 (Extended Data Figure 6a), exhibiting upregulation of Trm-associated genes and
296 downregulation of genes typically repressed in Trm cells. To confirm our transcriptional
297 data corresponded with surface protein expression, we assessed the levels of CXCR6
298 and CD69 co-expression on PEPCK cells during experimental VL. At day 56 p.i., we
299 identified a population of CXCR6$^+$ CD69$^+$ PEPCK cells in both the spleen and liver, with
300 an average frequency almost two-fold greater in the liver. This difference became more
301 pronounced following AmBisome treatment, resulting in an almost ten-fold increase in the
302 liver, compared to the frequency observed in the spleen (Figure 4c & d). These data
303 indicate that a subset of PEPCK cells acquires a Trm-like phenotype during experimental
304 VL in both the spleen and liver, with AmBisome treatment promoting their accumulation
305 in the liver.

306 We next compared the characteristics of Trm-like PEPCK cells in the spleen and liver to
307 assess potential tissue-specific differences in their phenotype and function. Upon
308 subclustering these cells, we observed distinct positional differences on the UMAP
309 between spleen and liver PEPCK cells (Figure 4e). Clustering analysis revealed three
310 clusters (Figure 4f), which were found in both tissues and across both control and
311 AmBisome-treated mice, though their frequencies varied. Among splenic Trm-like
312 PEPCK cells, the majority (64%) were in Cluster 2, while hepatic PEPCK cells were

313 predominantly (67%) in Cluster 1. The marker genes for Cluster 1 included *Xcl1*, *Il2*,
314 *Zfp683*, and *Tnf*, whereas Cluster 2 was enriched for *Il10*, *Ccr3*, *Sell*, and *Klf3* (Figure
315 4h). Additionally, , we found that Ambisome treatment also affected the Trm-like cell
316 phenotype (Figure 4i). Differential gene expression analysis revealed upregulation of
317 exhaustion-associated genes in control Trm-like PEPCK cells, including *Lag3*, *Il21*,
318 *Pdcd1*, and *Tigit*, while genes associated with enhanced function, such as *Il7r*, *Cxcr3*,
319 *Cd226*, and *Ifnar2*, were upregulated in Trm-like PEPCK cells from AmBisome-treated
320 mice (Extended Data Figure 6b). These data indicate that although Trm-like PEPCK cells
321 develop in both the spleen and liver, there are distinct transcriptional differences between
322 these cells in each tissue, with drug treatment further modulating their phenotype and
323 gene expression profiles.

324 Next, we compared the functional potential of Trm-like PEPCK cells in the spleen and
325 liver, as well as the behaviour of this $CD4^+$ T cell subset upon antigen re-exposure. After
326 *in vitro* stimulation with PMA and ionomycin, IFNγ production was similar between $CD69^-$
327 and $CD69^+$ PEPCK cells at day 56 p.i. in both tissues. However, *in vitro* IL-10 production
328 was significantly increased in $CD69^+$ PEPCK cells from AmBisome-treated mice (Figure
329 4j and k), independent of co-inhibitory receptor or chemokine receptor expression
330 (Extended Data Figure 6d). Interestingly, following rechallenge, $CD69^+$ PEPCK cells from
331 AmBisome-treated mice no longer produced IL-10 but instead exclusively produced IFNγ
332 (Figure 4j).In addition, while the frequencies of Trm-like PEPCK cells in both the spleen
333 and liver decreased following rechallenge, the total numbers of Trm-like PEPCK cells
334 increased in both organs (Extended Data Figure 6d). These data indicate that the
335 functional response of Trm-like PEPCK cells differ between the spleen and liver, with
336 hepatic Trm-like PEPCK exhibiting a regulatory-phenotype in AmBisome treated mice,
337 which then shifts towards an effector phenotype upon antigen re-exposure.

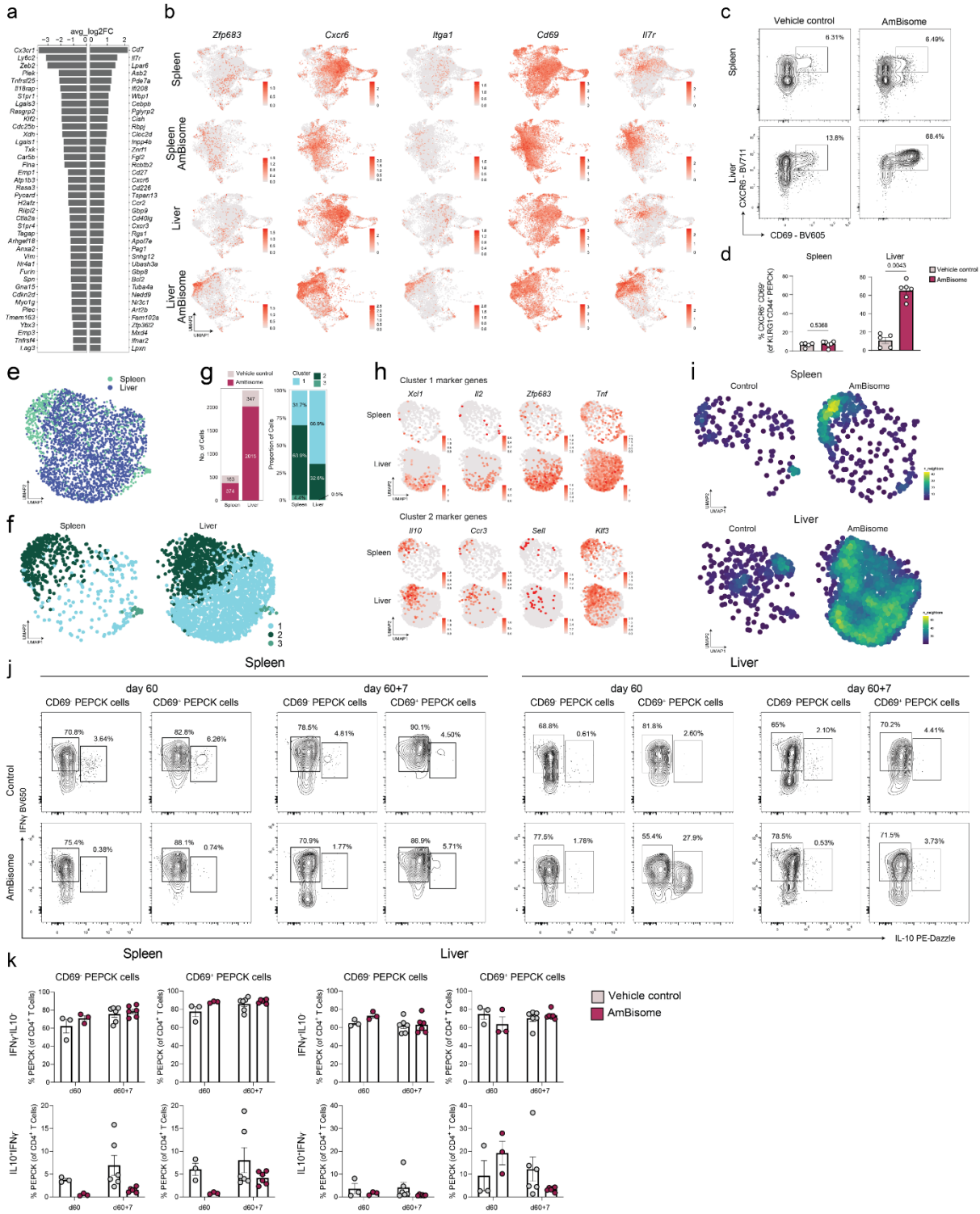


***Figure 4. AmBisome treatment promotes the development of hepatic Trm-like CD4⁺ T cells.*** ***(a)*** *Waterfall plot showing the top 40 up- and down-regulated marker genes for Cluster 5, identified using the 'FindAllMarkers()" function in Seurat.* ***(b)*** *UMAP visualisations of PEPCK cells subsetted by organ and treatment from d14-56 p.i. showing the expression of tissue-resident memory (Trm)*

*associated genes.* ***(c)*** *Flow cytometry plots showing CXCR6 and CD69 expression on PEPCK cells (gated on KLRG1$^{-}$CD44$^{+}$ PEPCK cells) from the spleen and liver at day 56 p.i. in experimental VL and* ***(d)*** *bar graphs showing the corresponding frequencies. Data is representative of two independent experients (n = 6 mice per group per experiment). Statistical testing was performed using two-tailed Mann-Whitney U test. Error bars represent mean ± SEM.* ***(e)*** *UMAP visualisation showing PEPCK cells from Cluster 5 after subsetting and data coloured by tissue of origin.* ***(f)*** *Three subsets of Trm-like PEPCK were identified after unsupervised clustering.* ***(g)*** *Bar graphs show the total number of cells in Cluster 5 from the spleen and liver as well as the proportion of cells in each cluster for each tissue.* ***(h)*** *UMAP visualisations showing selected marker genes for Clusters 1 and 2.* ***(i)*** *Density plot showing the distribution of control and AmBisome-treated samples for the spleen and liver.* ***(j*** *and* ***k)*** *Analysis of ex vivo IFNγ and IL-10 production by CD69$^{-}$ and CD69$^{+}$ PEPCK cells from the spleen and liver after PMA and ionomycin restimulation in vitro at day 60 and 7 days post-rechallenge (d60+7). Experiment performed once (n=3 mice per group for d60, n = 6 mice per group for d60+7).*

### ***Bhlhe40*** **promotes effector CD4$^{+}$ T cell function while suppressing CD4$^{+}$ T cell stemness.**

The clustering analysis in Figure 2 suggested there were limited changes in the CD4$^{+}$ T cell population structure dependent on tissue environment. However, to uncover gene expression patterns that were tissue-specific within clusters, differential gene expression analysis was performed between PEPCK cells from the spleen and liver at each time point in control-treated mice for the three largest clusters (Clusters 1 – 3). We identified 451, 391 and 282 differentially expressed genes in Cluster 1, 2 and 3, respectively (Extended Data Figure 8). These findings suggest that while the overall composition of CD4$^{+}$ T cells is largely comparable between tissues, local microenvironmental factors may contribute to subtle gene expression differences within specific CD4$^{+}$ T cell subsets, potentially influencing functional specialisation and immune dynamics in VL.

One of the genes that we identified as consistently upregulated in PEPCK cells from the spleen compared to the liver in Clusters 1, 2 and 3 was *Bhlhe40*, a transcription factor known to regulate T cell differentiation and inflammatory responses[29]. Given its established role in regulating the production of IFN-γ and IL-10 in various infection models[30,31,32,33] we focused on *Bhlhe40* to investigate its contribution to CD4$^{+}$ T cell fate decisions in experimental VL. We first examined the role of *Bhlhe40* in regulating the production of IFNγ and IL-10 by CD4$^{+}$ T cells *in vitro*. We employed CRISPR/Cas9 to target *Bhlhe40* in CD4$^{+}$ T cells from triple reporter (*Il10$^{gfp}$* x *Ifng$^{yfp}$* x *Foxp3$^{rfp}$*) C57BL/6

358 mice (Extended Data Figure 8a). Unstimulated CD4$^+$ T cells were targeted with *Bhlhe40*
359 sgRNA (*Bhlhe40*$^{KO}$ CD4$^+$ T cells), or a non-specific sgRNA as a control (*Bhlhe40*$^{WT}$ CD4$^+$
360 T cells), and then cultured under neutral (Th0), Th1 or Tr1 cell polarising conditions.
361 Successful editing of *Bhlhe40* in *Bhlhe40*$^{KO}$ CD4$^+$ T cells was confirmed by RT-qPCR
362 analysis. Targeting *Bhlhe40* did not effect the expression of *Maf* or *Prdm1*, genes
363 associated with Tr1 cell differentiation[14,16] (Extended Data Figure 8b), suggesting that the
364 loss of *Bhlhe40* does not influence these key regulatory transcription factors. However,
365 when we assessed cytokine production, although we observed no significant change in
366 IFNγ production, *Bhlhe40* deficiency caused a marked increase in IL-10 production in the
367 Tr1-stimulation condition (Extended Data Figure 8c). Further, flow cytometry analysis
368 revealed that the loss of *Bhlhe40* in CD4$^+$ T cells resulted in an increased frequency of
369 cells co-expressing both IFNγ and IL-10 (*IFNγ*$^+$*IL-10*$^+$), as well as a higher frequency of
370 cells expressing IL-10 alone (*IFNγ*$^-$*IL-10*$^+$) under Tr1 cell conditions. In contrast, the
371 frequency of IFNγ$^+$IL-10$^-$ CD4$^+$ T cells was reduced in both the Th1 and Tr1 cell
372 conditions.

373 To examine whether *Bhlhe40* played a role in determining tissue-specific outcomes of *L.*
374 *donovani* infection, wild type (WT) and *Bhlhe40*-deficient (*Bhlhe40*$^{-/-}$) mice were infected
375 and parasite burdens and immune responses assessed in the spleen and liver at day 14
376 p.i.. In the absence of *Bhlhe40*, we observed a significant increase in parasite burdens in
377 the liver and spleen, though the increase was more modest in the spleen (Figure 5a).
378 Additionally, although spleen organ weight was significantly reduced in *Bhlhe40*$^{-/-}$ mice
379 (Extended Data Figure 8f), no differences in total cell numbers were detected in the
380 spleen. In contrast, the liver of *Bhlhe40*$^{-/-}$ mice showed a notable decrease in total cell
381 numbers at day 14 p.i., suggesting that *Bhlhe40* may play a critical role in regulating
382 immune cell recruitment, effector functions and/or survival in the liver during infection.

383 Next, we evaluated the impact of *Bhlhe40* deficiency on the development of Th1
384 (IFNγ$^+$Tbet$^+$) and Tr1 (IFNγ$^+$IL-10$^+$) cells in experimental VL. Compared to WT mice,
385 *Bhlhe40*$^{-/-}$ mice exhibited a significant reduction in the frequency of Th1 cells in the liver
386 at day 14 p.i., while no such change was observed in the spleen (Figure 5c). In contrast,
387 *Bhlhe40*$^{-/-}$ mice displayed an increased frequency of Tr1 cells in both the spleen and liver

388 at this time point (Figure 5d). As might be expected, these changes were reflected in
389 significant alterations in the Th1:Tr1 cell ratios in both organs (Extended Data Figure 8g),
390 suggesting that *Bhlhe40* plays a critical role in regulating the balance between Th1 and
391 Tr1 cell responses during experimental VL. In *Bhlhe40*$^{-/-}$ mice, we also observed
392 suppression of TCF1$^{+}$ CD44$^{+}$ CD4$^{+}$ T cell development in the spleen at day 14 p.i. (Figure
393 5e), consistent with previous findings indicating a role for this transcription factor in CD4$^{+}$
394 T cell lineage commitment towards stemness[34]. *Bhlhe40* deficiency also impaired the
395 development of central memory CD4$^{+}$ T cells in both the spleen and liver at this time point
396 (Figure 5f). Conversely, *Bhlhe40*$^{-/-}$ mice exhibited an increase in effector memory CD4$^{+}$ T
397 cell development in the liver (Figure 5g), supporting an important role for *Bhlhe40* the
398 development of central memory and stem-like CD4$^{+}$ T cells during experimental VL.

399 To establish cell intrinsic roles for *Bhlhe40* in CD4$^{+}$ T cells during experimental VL, we
400 performed CRISPR/Cas9 editing of PEPCK cells targeting *Bhlhe40*
401 (PEPCK$^{\Delta Bhlhe40}$)(Figure 5h). Compared to control PEPCK (PEPCK$^{WT}$) cells, the frequency
402 of PEPCK$^{\Delta Bhlhe40}$ cells was significantly reduced in both the spleen and liver,
403 suggesting*Bhlhe40* may play a role in the expansion and/or survival of CD4$^{+}$ T cells
404 (Figure 5i). Flow cytometry analysis revealed a marked decrease in IFNγ$^{+}$IL-10$^{-}$ PEPCK
405 cells in the absence of *Bhlhe40* in both organs, while IFNγ$^{-}$IL-10$^{+}$ PEPCK cells were
406 significantly increased in the liver but remained unchanged in the spleen (Figure 5j). No
407 differences were observed in the frequency of IFNγ$^{+}$IL-10$^{+}$ PEPCK cells. However, the
408 loss of *Bhlhe40* resulted in a higher proportion of TCF1$^{+}$ PEPCK cells in both the spleen
409 and liver, accompanied by a reduction in CXCR6 and KLRG1 expression (Figure 5k).
410 Together, these findings suggest that *Bhlhe40* regulates the balance between IFNγ and
411 IL-10 production by CD4$^{+}$ T cells, promotes effector cell differentiation and function, and
412 suppresses either the development or maintenance of stem-like CD4$^{+}$ T cells in
413 experimental VL.

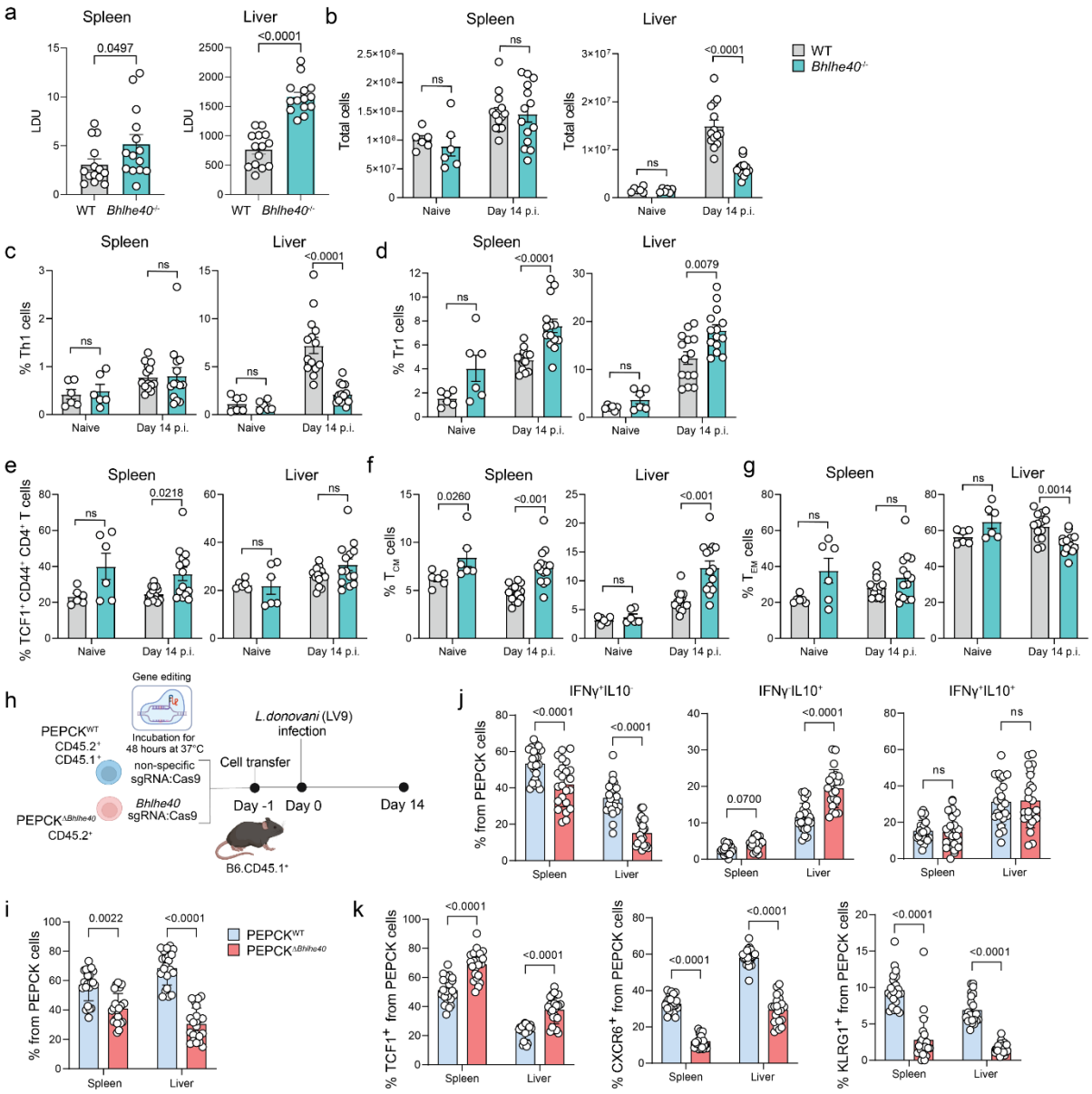


***Figure 5. Bhlhe40 drives effector CD4⁺ T cell fate while restricting stemness in experimental VL. (a)*** *Wildtype (WT) and Bhlhe40$^{-/-}$ mice were infected with L. donovani and parasite burdens were measured in the spleen and liver at day 14 p.i.. LDU, Leishman-Donovan units.* ***(b)*** *Total number of cells in the livers of naïve mice and infected mice at day 14 p.i.* ***(c)*** *Frequency of Th1 cells (IFNγ$^{+}$Tbet$^{+}$CD4$^{+}$ T cells),* ***(d)*** *Tr1 cells (IFNγ$^{+}$IL-10$^{+}$ CD4$^{+}$ T cells),* ***(e)*** *TCF1$^{+}$CD44$^{+}$ CD4$^{+}$ T cells,* ***(f)*** *central memory T cells (Tcm; CCR7$^{+}$CD44$^{+}$ CD4$^{+}$ T cells), and (g) effector memory T cells (Tem; CCR7$^{-}$CD44$^{+}$ CD4$^{+}$ T cells) in the spleen and liver of naïve and infected mice at day 14 p.i.. Statistical testing was performed using two-tailed Mann-Whitney U test. Error bars represent ± SEM. Data are pooled from two experiments, where n = 6 naïve WT and Bhlhe40$^{-/-}$ mice, and n = 14 WT and Bhlhe40$^{-/-}$ mice at day 14 p.i..* ***(h)*** *CRISPR/cas9 editing of PEPCK cells targeting Bhlhe40 (PEPCK$^{\Delta Bhlhe40}$), or a non-specific guide RNA (PEPCK$^{WT}$), was performed and cells were subsequently co-transferred into B6.CD45.1$^{+}$ mice, which were then*

*infected with L. donovani. Flow cytometry assessment of PEPCK cells was performed at day 14 p.i.. **(i)** Graph showing the frequency of PEPCK$^{WT}$ and PEPCK$^{\Delta Bhlhe40}$ cells at day 14 p.i. from the spleen and liver. **(j)** Graphs showing the percentage of IFNγ and IL-10 production by PEPCK$^{WT}$ and PEPCK$^{\Delta Bhlhe40}$ cells after in vitro stimulation with PMA and ionomycin at day 14 p.i. from the spleen and liver. **(k)** Graphs showing the expression of TCF1, CXCR6 and KLRG1 in PEPCK$^{WT}$ and PEPCK$^{\Delta Bhlhe40}$ cells at day 14 p.i. from the spleen and liver. **(i-k)** Statistical testing was performed using two-way ANOVA with Sidak's multiple comparisons test. Error bars represent mean ± SEM. Data are pooled from four independent experiments, with n = 5/6 mice per group per experiment.*

414 ***Tcf7*-expressing CD4$^+$ T cells exhibit transcriptional characteristics associated with**
415 **stemness in experimental VL.**

416 Stem-like CD4$^+$ T cells represent an important memory cell population that reside in
417 secondary lymphoid tissues, with a unique capacity to replenish effector T cells and
418 sustain long-term immunity[35,36,37,38]. The clustering analysis in Figure 2 identified Cluster
419 7 as a spleen-specific CD4$^+$ T cell subset characterised by *Tcf7* expression. Given the
420 association of *Tcf7* with stem-like CD4$^+$ T cells, we investigated whether this subset
421 functions as a progenitor population capable of sustaining effector responses during
422 chronic VL.To address this, we analysed the transcriptional and phenotypic
423 characteristics of Cluster 7, assessing the self-renewal potential and differentiation
424 capacity for this CD4$^+$ T cell subset.

425 First, we examined the transcriptional and phenotypic characterisitics of Cluster 7 in more
426 detail and observed expression of *Tcf7, Ccr7, Lef1, Cxcr5, Il7r,* and *Slamf6*, canonincal
427 genes associated with stemness[35,39] (Figure 6a). Several of these genes overlapped with
428 the top marker genes that were differentially upregulated in this cluster (Figure 6b). In
429 addition, when compared to a stem-like CD8$^+$ T cell gene signature, we saw enriched
430 expression of this signature in Cluster 7, and a corresponding downregulated effector
431 CD8$^+$ T cell gene signature (Extended Data Figure 9a). Together, these data suggest that
432 Cluster 7 PEPCK cells exhibit a stem-like transcriptional profile.

433 Stem-like CD8$^+$ T cells are a heterogeneous population[40], so to examine whether similar
434 diversity existed in stem-like PEPCK cells, we performed subclustering analysis. Three
435 distinct clusters of stem-like PEPCK cells were identified (Extended Data Figure 9b),
436 which exhibited a strong association with treatment type (Extended Data Figure 9c). At

437 day 14 p.i., the majority of stem-like PEPCK cells originated from the spleen and were
438 predominantly found in Cluster 2 (Extended Data Figure 9d). Beyond this time point, the
439 number of splenic stem-like PEPCK cells declined significantly, except in AmBisome-
440 treated mice where their frequencies remained stable. Consistent with this, flow cytometry
441 analysis confirmed that the frequency of stem-like PEPCK cells in the spleen was
442 maintained in AmBisome-treated mice, whereas they declined in vehicle-treated mice
443 after day 14 p.i. (Extended Data Figure 9e). While these stem-like PEPCK cells persisted
444 in the spleen following AmBisome treatment, their transcriptional profile shifted, with cells
445 primarily transitioning to Cluster 1. Assessment of cluster marker genes identified Cluster
446 1 cells to be associated with self-renewal and longevity (*Il7r, S100a4, Klf6, Bcl2*)[41]
447 (Extended Data Figure 9f). In contrast, Cluster 2 marker genes associated with activation
448 and exhaustion (*Klrb1c, Il21, Lag3, Bcl6*), indicating a subset prone to functional decline.
449 These data suggest that AmBisome treatment not only preserves splenic stem-like
450 PEPCK cells but also supports their transition into a transcriptional state favoring long-
451 term persistence rather than exhaustion.

452 Given the similarities between stem-like T cells and central memory T cells (Tcm), we
453 examined whether there was overlap between stem-like PEPCK cell clusters and Tcm
454 cells. Classical Tcm cells express *Sell* and *Ccr7*, enabling lymphoid circulation, but most
455 stem-like PEPCK cells lacked *Sell* expression (Extended Data Figure 9g), suggesting
456 they do not fully align with a Tcm identity. The expression of *Mki67* by stem-like PEPCK
457 cells also indicates an actively cycling state rather than a quiescent Tcm cell state. While
458 Cluster 3 showed the closest resemblance to Tcm due to its expression of *Ccr7* and Sell.
459 However, this cluster constituted only ~2% of the total stem-like population, indicating that
460 these cells are rare, and their low frequency makes definitive classification as
461 conventional Tcm challenging.

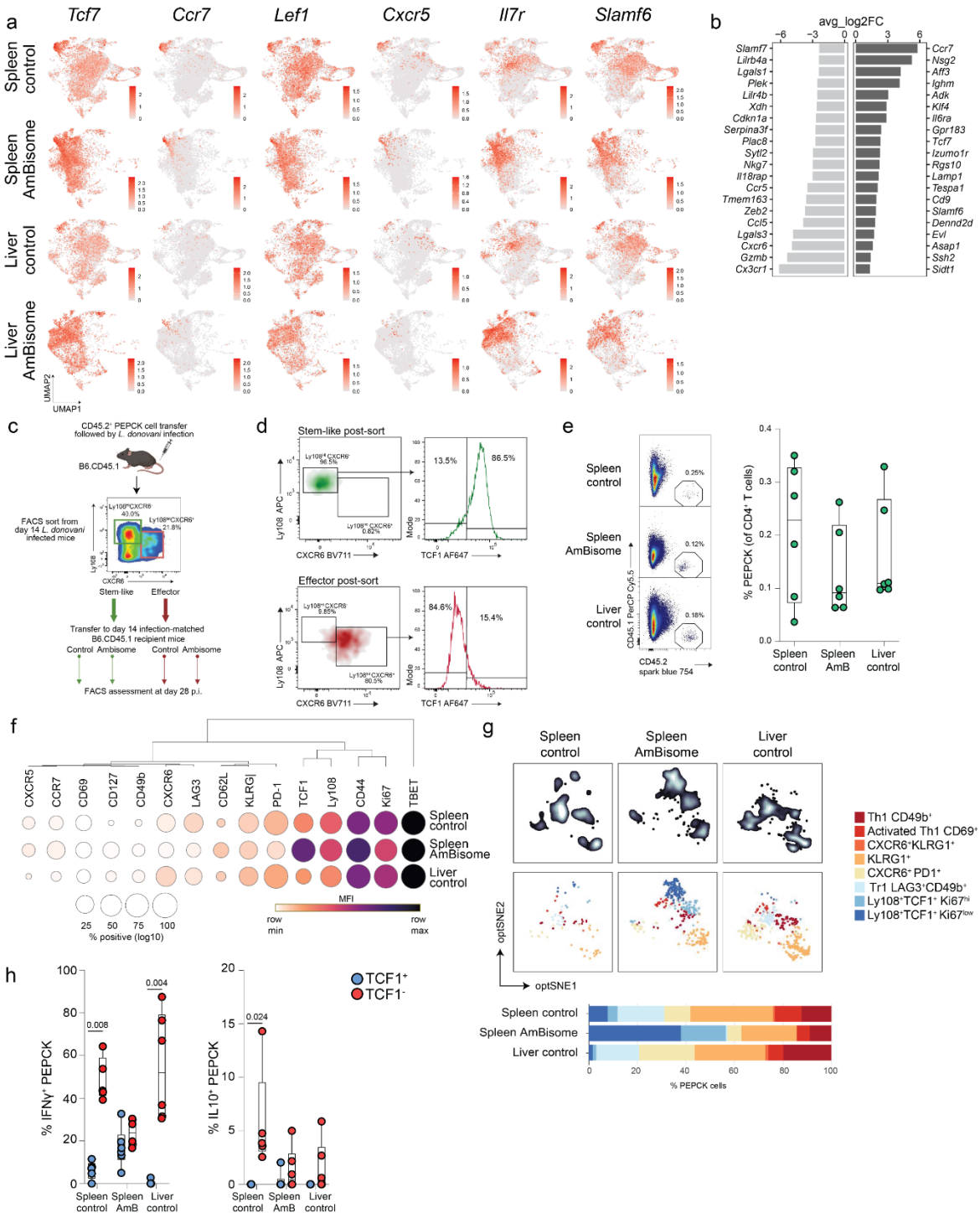


***Figure 6. Tcf7-expressing CD4⁺ T cells exhibit stem-like properties in experimental VL. (a)*** *UMAP visualisations of PEPCK cells subsetted by organ and treatment from d14-56 p.i. showing the expression of stemness-associated genes.* ***(b)*** *Waterfall plot showing the top 20 up- and down-regulated marker genes for Cluster 7, identified using the "FindAllMarkers()" function in Seurat.* ***(c)*** *Stem-like (Ly108$^{hi}$Cxcr6$^{-}$) and effector (Ly108$^{int}$CXCR6$^{+}$) PEPCK cells were isolated from the spleens of L. donovani infected mice at day 14 p.i. and adoptively transferred into*

*infection matched mice that had been treated with vehicle control (control) or Ambisome (AmB) the day prior, followed by flow cytometry assessment at day 28 p.i.. **(d)** Flow cytometry plots showing the expression of TCF1 on isolated stem-like and effector PEPCK cells. **(e)** Representative flow cytometry plots and graph showing the frequency of PEPCK cells at day 28 p.i.. **(f)** The average expression (as MFI) and percentage (as positive events) is summarized in dot-plot format for PEPCK cells at day 28 p.i.. **(g)** optSNE visualisation showing PEPCK cell distribution and FlowSOM clustering (top) and the frequency of identified clusters for each sample (bottom). **(h)** Graphs showing the frequency of IFNγ and IL-10 producing TCF1$^{+}$ and TCF1$^{-}$ PEPCK cells after in vitro stimulation with PMA and ionomycin. Statistical analysis was performed using multiple Mann-Whitney U tests. Data are from one experiment, with n = 5/6 mice per group.*

**Splenic stem-like CD4$^{+}$ T cells help sustain effector responses during chronic infection in experimental VL.**

To further investigate the role of *Tcf7* in CD4$^{+}$ T cells, we used CRISPR/Cas9-mediated gene editing to disrupt *Tcf7* in PEPCK cells. Wild-type (PEPCK$^{WT}$) and *Tcf7*-edited (PEPCK$^{\Delta Tcf7}$) PEPCK cells were co-transferred into recipient mice, which were subsequently infected with *L. donovani* (Extended Data Figure 9h). Fourteen days post-infection, we assessed the impact of *Tcf7* deletion on PEPCK cell persistence and phenotype using flow cytometry. Surprisingly, we observed no significant differences between PEPCK$^{WT}$ and PEPCK$^{\Delta Tcf7}$ cells in terms of frequency or survival (Extended Data Figure 8i). While most surface marker expression remained unchanged between PEPCK$^{WT}$ and PEPCK$^{\Delta Tcf7}$ cells, we did observe slightly increased CXCR6 expression, and reduced KLRG1 expression in PEPCK$^{\Delta Tcf7}$ cells compared to the PEPCK$^{WT}$ cells (Extended Data Figure 8j). However, by knocking out *Tcf7* prior to infection, we may have allowed *Tcf7*-independent pathways to emerge to drive CD4$^{+}$ T cell expansion and effector responses.

Therefore, to directly assess the self-renewal potential and differentiation capacity of stem-like CD4$^{+}$ T cells, we employed an adoptive transfer model using stem-like and effector PEPCK cells. For this, we transferred PEPCK cells (CD45.2$^{+)}$ into B6.CD45.1$^{+}$ mice and subsequently infected them with *L. donovani*. On day 14 p.i., when splenic stem-like PEPCK cells had established, we isolated stem-like (Ly108$^{hi}$Cxcr6$^{-}$), where we used Ly108 as a surrogate for TCF1 expression[38], and effector (Ly108$^{int}$Cxcr6$^{+}$) PEPCK cells from the spleens of these mice (Figure 6c). The expression of TCF1 by stem-like PEPCK cells was confirmed by flow cytometry (Figure 6d) prior to adoptively transferring both

485 stem-like and effector PEPCK cells into separate groups of infection matched B6.CD45.1
486 recipient mice that had either been treated with vehicle control or AmBisome on the day
487 prior. After 14 days, we then performed flow cytometry assessment of PEPCK cells from
488 these recipient mice. PEPCK cells were identified in the spleens and livers of mice that
489 had received stem-like PEPCK cells, except in the livers of AmBisome-treated mice,
490 where only few PEPCK cell numbers were observed (Figure 6e). In contrast, no PEPCK
491 cells were detected in the spleen or liver of mice that had received the effector PEPCK
492 cells. These findings suggest that TCF1 expression is essential for the self-renewal and
493 maintenance of these cells, which in turn, differentiate into effector $CD4^+$ T cells.

494 Surface marker analysis confirmed that PEPCK cells from all three groups where they
495 could be readily detected, exhibited a Th1 cell phenotype, marked by Tbet expression,
496 and were actively proliferating, as indicated by Ki67 expression (Figure 6f). In both the
497 spleen and liver, PEPCK cells from vehicle control-treated mice displayed higher
498 expression of Lag3 and PD-1 compared to those from AmBisome-treated mice. Notably,
499 splenic PEPCK cells from AmBisome-treated mice retained a stem-like phenotype,
500 characterised by TCF1 expression. To further define these populations, unsupervised
501 clustering of PEPCK cell FACS data identified eight distinct clusters (Figure 6g). These
502 included five effector-like clusters ($Cd49b^+$, $CD69^+$, $CXCR6^+KLRG1^+$, $KLRG1^+$ and
503 $CXCR6^+PD1^+$), a regulatory cluster (Tr1 $LAG3^+CD49b^+$) and two stem-like clusters
504 ($Ly108^+TCF1^+Ki67^{hi}$, $Ly108^+TCF1^+Ki67^{low}$), distinguished by their Ki67 expression levels.
505 While all clusters were present across treatment groups, their frequencies differed (Figure
506 6g). Notably, AmBisome-treated mice exhibited an increased proportion of splenic stem-
507 like PEPCK cells compared to vehicle control treated mice, with a significant enrichment
508 of the $Ly108^+TCF1^+Ki67^{low}$ subset, indicative of a more quiescent phenotype. Consistent
509 with this, functional analysis of PEPCK cells following *in vitro* stimulation with PMA and
510 ionomycin revealed that $TCF1^+$ PEPCK cells produced little to no IFNγ or IL-10, whereas
511 $TCF1^-$ PEPCK cells readily produced these cytokines (Figure 6h). These findings suggest
512 that stem-like PEPCK cells in the spleen remain in a functionally quiescent state, with
513 AmBisome treatment promoting their maintenance as a long-term reservoir that may
514 sustain immune responses in experimental VL.

515 **Discussion**

516 Effective CD4$^+$ T cell responses are critical for immunity to VL, yet the factors shaping
517 their differentiation and function across distinct tissue environments remain poorly
518 understood. Here, we explored how CD4$^+$ T cells adapt to the contrasting immune
519 landscapes of the spleen and liver during experimental VL, uncovering key differences in
520 their composition, transcriptional profiles and functional states. By integrating single-cell
521 transcriptomics with complementary analyses, we captured the heterogeneity of these
522 responses and identified key transcriptional programs associated with effector function,
523 regulatory potential and stem-like properties. Furthermore, we examined how anti-
524 parasitic treatment with AmBisome influences CD4$^+$ T cell dynamics, shedding light on
525 mechanisms that likely contribute to long-term immunity in VL. Together, these findings
526 offer a detailed framework for understanding tissue-specific immunity in VL and provide
527 insights relevant to both therapeutic interventions and vaccine development.

528 CD4$^+$ T cells are essential for resolving *L. donovani* infection, with the balance between
529 Th1 and Tr1 cells often considered a key determinant of disease outcome[42]. However,
530 our study provides the first in-depth, high-resolution analysis of CD4$^+$ T cell responses in
531 experimental VL, revealing that CD4$^+$ T cell heterogeneity extends far beyond this
532 conventional Th1-Tr1 cell framework. Rather than being a simple binary, we uncovered
533 a diverse spectrum of transcriptional states that shape immunity and disease progression
534 in a more nuanced and tissue-specific manner. We identified multiple Th1 cell subtypes,
535 including effector, memory-like, regulatory and stem-like subsets, underscoring a broader
536 spectrum of Th1 cell functional states than previously appreciated. While the classification
537 of CD4$^+$ T cells into distinct subsets such as Th1, Th2, Th17, Tfh and Treg cells is well
538 established[10], it is increasingly recognised that heterogeneity exisits within these broad
539 categories. Studies on Th17 and Tfh cells have particularly highlighted the existence of
540 distinct functional subpopulations with different transcriptional programs and
541 capacities[43,44]. However, the diversity within the Th1 cell lineage has remained less well
542 explored. CD4$^+$ T cells exhibit phenotypic plasticity, often co-expressing transcriptional
543 programs associated with multiple cell subsets[45,46], and our findings suggest that such
544 flexibility extends to Th1 cells in the context of VL. This highlights the need to consider

545 how different Th1 cell subsets, and their balance, contribute to immune responses in
546 chronic infection settings.

547 The similarity between polyclonal *Leishmania*-specific CD4$^+$ T cells and monoclonal
548 PEPCK cells in our study suggests that TCR diversity does not predominantly dictate
549 tissue localisation or differentiation patterns in experimental VL. This observation aligns
550 with findings in other chronic infections, such as lymphocytic choriomeningitis virus
551 (LCMV)[47,48], where CD4$^+$ T cells exhibit functional plasticity irrespective of their TCR
552 specificity. These insights underscore the significance of tissue-specific
553 microenvironmental factors, such as cytokine milieu, stromal interactions, and metabolic
554 conditions in guiding CD4$^+$ T cell differentiation and localisation. Consequently,
555 therapeutic strategies that modulate these extrinsic factors may be more effective in
556 shaping protective immunity in VL.

557 Our analysis revealed striking transcriptional similarities between CD4$^+$ T cells from the
558 spleen and liver, challenging our initial hypothesis that intrinsic differences in these cells
559 drive the disparity in parasite control between these organs in experimental VL. Instead,
560 our findings suggest that extrinsic factors within the tissue microenvironment likely play a
561 more dominant role. The spleen undergoes profound structural changes during chronic
562 infection, including splenomegaly and loss of lymphoid tissue organisation[17,18,19]. In
563 contrast, the liver mounts a granulomatous response that effectively contains infection.
564 This breakdown in splenic architecture, driven in part by excessive TNF signaling and IL-
565 10 induction[49], likely contributes to the failure of parasite control in the spleen despite the
566 presence of transcriptionally similar CD4$^+$ T cell populations in both organs.
567 Understanding the localisation of CD4$^+$ T cell subsets within the spleen during infection
568 could provide key insights into how their interactions with other immune cells and stromal
569 networks become disrupted, ultimately impairing their ability to effectively clear parasites.

570 Although broad transcriptional differences between the spleen and liver were limited, we
571 identified shifts in subset frequencies, including the presence of a novel stem-like CD4$^+$
572 T cell population in the spleen. Stem-like T cells support sustained immune responses
573 and retain the capacity to differentiate into diverse effector subsets[35,37]. However,
574 *Bhlhe40*, identified as upregulated in the spleen, emerged as a key suppressor of this

575 phenotype. *Bhlhe40* deficiency skewed CD4$^+$ T cell responses, reducing Th1 cell
576 differentiation while promoting Tr1 cells, as has previously been reported in *Toxoplasma*
577 *gondii* and *Mycobacterium tuberculosis* infection[30,33]. This also correlated with impaired
578 parasite control in the liver and spleen in experimental VL. Additionally, *Bhlhe40* restricted
579 TCF1 expression, thereby influencing stem-like CD4$^+$ T cell development. This raises the
580 possibility that *Bhlhe40* regulates the persistence and function of TCF1$^+$ PEPCK cells,
581 with broader implications for T cell fate decisions in chronic infection. These findings
582 highlight the complexity of CD4$^+$ T cell differentiation in VL, suggesting that tissue-specific
583 cues shape not only effector responses but also the balance between renewal and
584 exhaustion.

585 The most profound transcriptional shift in CD4$^+$ T cells occurred following AmBisome
586 treatment, an observation with important implications for VL immunity. In human VL,
587 patients who recover often exhibit long-term resistance to reinfection, highlighting the
588 need to understand how the immune landscape is reshaped post-treatment. In our model,
589 AmBisome treatment preserved the stem-like CD4$^+$ T cell population while also promoting
590 the development of Trm-like CD4$^+$ T cells. Trm cells provide rapid localised immune
591 responses upon pathogen re-exposure[50], and their presence likely contributes to effective
592 immunity against *L. donovani* infection. Defining the roles of these populations in VL
593 immunity will be critical for guiding future therapeutic and vaccine strategies.
594 Understanding how treatments like AmBisome modulate the immune landscape can
595 inform the development of interventions that not only clear the infection but also establish
596 robust, long-lasting immunity.

597 Together, our findings provide a comprehensive view of the complexity of CD4$^+$ T cell
598 responses in experimental VL, revealing a previously unappreciated heterogeneity in Th1
599 cell subsets and highlighting the critical influence of the tissue microenvironment, infection
600 stage, and drug treatment on their differentiation and function. The observation that CD4$^+$
601 T cells from the spleen and liver share highly similar transcriptional profiles challenges
602 traditional assumptions about organ-specific immune programming and suggests that
603 extrinsic factors, rather than intrinsic differences in T cells, drive the disparate control of
604 *Leishmania donovani* between these tissues. The identification of stem-like PEPCK cells

605 and their persistence following drug treatment raises intriguing questions about their role
606 in long-term immunity and whether they can be harnessed for therapeutic benefit.
607 Furthermore, the promotion of Trm-like cell populations post-treatment underscores the
608 potential for tissue-resident memory responses to contribute to durable immunity in VL.
609 The involvement of transcriptional regulators such as Bhlhe40 in shaping these immune
610 dynamics presents an exciting avenue for future research, particularly in understanding
611 how interventions might be tailored to optimise protective immunity while preventing
612 immune exhaustion. More broadly, these findings have implications beyond VL,
613 contributing to our understanding of how $CD4^+$ T cell heterogeneity and plasticity shape
614 immune responses in chronic infections. By dissecting the mechanisms that govern $CD4^+$
615 T cell fate decisions, we can refine immunotherapeutic strategies not only for
616 leishmaniasis but also for other persistent infections, autoimmune conditions, and vaccine
617 development.

618 **Materials and methods**

619 **Mice**

620 B6.CD45.1$^{+}$ (B6.SJL-Ptprc$^{a}$ Pepc$^{b}$/BoyJ) mice were purchased from Animal Resources
621 Centre/ Ozgene (Canning Vale), Bhlhe40$^{-/-}$ mice (B6.129S1(Cg)-*Bhlhe40$^{tm1.1Rhli}$*/MpmJ)
622 were purchased from The Jackson Laboratory, and C57BL/6J.PEPCK and B6.Rag1$^{-/-}$
623 mice were bred in house. C57BL/6-Il10tm1Flv/J (*Il10$^{gfp}$*; JAX:008379)[51], B6.129S4-
624 Ifngtm3.1Lky/J (*Ifng$^{yfp,}$* RRID: IMSR_JAX: 017581)[52] and C57BL/6-*Foxp3$^{tm1flv}$*/J (*Foxp3$^{rfp}$*;
625 JAX:008374) mice were crossed to produce a triple reporter strain. All mice were female,
626 aged 8-12 weeks, and maintained under specific pathogen-free conditions within the
627 animal facility at QIMR Berghofer. Mice were housed in exhaust-ventilated cages (Opti-
628 mice) with ≤6 mice per cage, and room temperature was maintained between 19 °C and
629 22 °C, with humidity between 55% and 65% and with 12-h/12-h dark/light cycle with a 15-
630 min sunrise and sunset. All animal procedures and protocols were in accordance with the
631 "Australian Code of Practice for the Care and Use of Animals for Scientific Purposes"
632 (Australian National Health and Medical Research Council [NHMRC]) and approved by
633 the QIMR Berghofer Animal Ethics Committee (Brisbane, Queensland, Australia;
634 approval number A1707-615M/A2305-606 or P2304/P3887).

635 **PEPCK adoptive transfer**

636 Spleens were collected from C57BL/6J.PEPCK mice and homogenised through a 100
637 µm cell strainer to create a single cell suspension. Red blood cells were lysed using Red
638 Blood cell Lysing Buffer Hybri-Max (Sigma-Aldrich) and samples were washed with 1%
639 FCS/PBS. Cells were enriched for CD4$^{+}$ T cells using EasySep™ Mouse CD4$^{+}$ T Cell
640 Isolation kits (Stemcell Technologies), according to the manufacturer's protocol. Naïve
641 PEPCK cells (CD62L$^{hi}$ CD44$^{lo}$) were isolated by flow cytometry and then transferred to
642 each mouse (1 x $10^{4}$ cells in 200 µl volume per mouse) via lateral tail vein intravenous
643 (i.v.) injection.

644 ***Leishmania donovani* infections in mice**

645 *Leishmania donovani* (LV9; MHOM/ET/67/HU3) parasites were maintained by passage
646 in B6.Rag1$^{-/-}$ mice and amastigotes were isolated from the spleens of chronically infected

647 mice, as previously described[26]. Mice were infected with 2 x $10^7$ LV9 amastigotes i.v. (in
648 200 µl volume) via the lateral tail vein.

649 **Quantifying *Leishmania* parasite burdens**

650 Spleen and liver impression smears were used to determine parasite burdens and were
651 expressed as Leishman Donovan Units (LDU; number of amastigotes per 1000 host
652 nuclei multiplied by the organ weight (in grams)).

653 **AmBisome drug treatment**

654 Liposomal amphotericin B (AmBisome®; Gilead Sciences) was prepared according to the
655 manufacturer's instructions. Mice were treated with a single dose of AmBisome (10 µg/g
656 body weight) or vehicle control (3.875% glucose (vol/vol)) at day 14 post-infection,
657 administered i.v. (200 µl volume per mouse) via the lateral tail vein.

658 **Preparation of spleen and liver single-cell suspensions**

659 Spleens were collected and homogenised through a 100-µm cell strainer to create a
660 single cell suspension. Red blood cells were lysed using Red Blood cell Lysing Buffer
661 Hybri-Max (Sigma-Aldrich) and samples were washed with 1% FCS/PBS. Cells were
662 resuspended in 1% FCS.PBS and counted using a Countess Cell Counting Chamber
663 Slides on the Countess II FL (Invitrogen), per the manufacturer's protocol. Cells were
664 enriched for $CD4^+$ T cells using EasySep™ Mouse $CD4^+$ T Cell Isolation kits (Stemcell
665 Technologies) or magnetic-activated cell sorting (MACS) using anti-mouse CD4
666 Microbeads (Miltenyi Biotec), according to the manufacturer's protocol.

667 Livers were first perfused via the hepatic portal vein with 1x PBS and then homogenized
668 through a 100-µm cell strainer to create a single cell suspension. Hepatocytes were
669 separated from leukocytes using a 33% (vol/vol) Percoll Density Gradient (GE
670 Healthcare). After removal of supernatant containing unwanted cells and debris, the liver
671 leukocyte pellet was processed as described above for the splenic tissue.

672 **Flow cytometry**

673 LIVE/DEAD™ Fixable Blue Dead Cell Stain Kit, for UV excitation (ThermoFisher
674 Scientific) was used as the initial step to exclude dead cells. Cells were then incubated

675 with 0.2µl/sample TruStain FcX™ PLUS (anti-mouse CD16/32) antibody (Biolegend) for
676 blocking of Fc receptors, CCR7-PeCy7 (Biolegend) was stained individually for 15
677 minutes at 37°C in the dark followed by surface staining with a combination of the
678 following antibodies; CD44 AF-700 or FITC (Biolegend), CD90.2 PerCP-Cy5.5
679 (Biolegend), CD127 BV421 (Biolegend), CD69 BV605 (Biolegend), CD62L BV650 or PE
680 (Biolegend), CXCR6 BV711 (Biolegend), CD45.2 Sparkblue-754 or PerCP-Cy5.5
681 (Biolegend), CD45.1 PerCP-Cy5.5 (Biolegend), KLRG1 PEDazzle-594 (Biolegend), PD1
682 APCFire-750 (Biolegend), Ly108 APC (Biolegend), CD4 BUV395 (BD Biosciences) or
683 AF647 (Biolegend), CXCR5 BV785 and TCRβ BUV737 (BD Biosciences), for 60 minutes
684 at 37°C in the dark.

685 For intracellular cytokine staining, cells were first stained with a mix of LAG3 BV785,
686 CCR2 BV421, CCR5 PerCP-Cy5.5 and CD49b PeCy7 for 30 minutes at 37°C in the dark
687 and then stimulated with a combination of 50ng/ml Phorbol-12-myristate-13-acetate
688 (PMA; Sigma Aldrich) and 1uM Ionomycin (Sigma Aldrich) for 3 hours at 37°C in the
689 presence of 1x Monensin (1000x Biolegend) or 1x Brefeldin A (1000x Biolegend) followed
690 by surface staining as above. Cells were then fixed and permeabilised with the
691 eBioscience™ Intracellular Fixation and Permeabilisation Buffer Set (Thermofisher),
692 according to the manufacturers' instructions, followed by staining for IL10 PE-Dazzle594
693 (Biolegend), IFNγ BV650 (BD), Foxp3 Ef450 (eBioscience), TCF1 PE (Cell Signaling
694 Technolgies), Tbet PE-Cy7 (Biolegend), Ki67 APC-fire 750 (Biolegend), CTLA4 BV650
695 (Biolegend) for 45 minutes at 37°C in the dark.

696 Data were acquired using a Cytek® Aurora spectral analyser (Cytek Biosciences). Data
697 were gated using FlowJo software (TreeStar) and analyzed with GraphPad Prism v9. For
698 clustering analysis the OMIQ™ (https://www.omiq.ai/) platform was used to batch correct
699 data with gaussNorm, followed by tSNE clustering and FlowSOM analysis to identify
700 unique clusters. Mean fluorescent intensity heat maps and expression dot plots were
701 made using MORPHEUS (https://software.broadinstitute.org/Morpheus) (Broad
702 Institute).

703 **Tetramer staining**

704 *Leishmania*-specific $CD4^+$ T cells were identified by staining with a MHC-class II I-$A^b$
705 $PEPCK_{335-351}$ APC-conjugated tetramer. To minimise unspecific binding of cells, cells
706 were also stained with a control human CLIP (I-$A^b$ $CLIP_{87-101}$) phycoerythrin (PE)–
707 conjugated tetramer. The tetramers were produced by the NIH Tetramer Core Facility and
708 cells were stained for 30 minutes at 37°C.

709 **Single-cell RNA capture and sequencing**

710 Single cell suspensions from mouse spleen and liver were prepared as described above.
711 Cells were then incubated with TruStain FcX™ PLUS (anti-mouse CD16/32) antibody
712 (BioLegend) for blocking of Fc receptors followed by surface staining with a combination
713 of surface antibodies (as listed in Supplementary Table 1) for 30 minutes on ice in the
714 dark. In addition, samples were also incubated with TotalSeq™-C anti-mouse Hashtag
715 antibodies (Biolegend; Supplementary Table 1) on ice for 30 minutes in the dark and
716 washed with 1% BSA.PBS. Cells were then resuspended in 1% BSA.PBS containing
717 SYTOX™ Blue Dead Cell Stain (ThermoFisher Scientific) at a dilution of 1:1000. PEPCK
718 cells ($CD4^+CD90.2^+CD45.2^+CD45.1^-$) were then sorted using a FACS ARIA III (BD) into
719 a 1% BSA.PBS buffer. After sorting, PEPCK cells were loaded onto a Chromium Single
720 Cell Chip (10x Genomics) for generation of gel bead-in emulsions (GEMs), according to
721 manufacturers' instructions, with a target capture rate of ~4000 single cells per sample.
722 Generation of cDNA and single-cell RNA sequencing libraries for Illumina sequencing
723 were generated using the Chromium Single Cell 5' v2 kit (10x Genomics). All samples
724 from a single time point were processed together in one well of the Chromium chip and
725 the resulting libraries were prepared in parallel. All libraries were pooled and sequenced
726 on five Illumina flow cells with a 10-base index read, a 26-base read 1 containing cell-
727 identifying barcodes and unique molecular identifiers (UMIs), and a 90-base read 2
728 containing transcript sequences on an Illumina NextSeq550.

729 **Single-cell RNA sequencing data processing and analysis**

730 Illumina FASTQ files were run through the 'cellranger count' pipeline from Cell Ranger
731 v6.0.1 (10x Genomics) with 10x Genomics mouse genome mm10-2020-A as a reference.
732 *Seurat* v4[53] was used for downstream analysis. Only genes expressed in three or more
733 cells were considered. Cells were filtered to remove those expressing fewer than 200

genes and more than 5000 genes, and those with more than 10% mitochondrial content. Cells identified as doublets were removed by demultiplexing based on HTO using "HTODemux()" function from *Seurat* package. To minimise TCR-driven variability in clustering, T cell receptor alpha and T cell receptor beta genes were removed prior to downstream analysis. Additionally, a cluster of contaminating hepatocytes was excluded from the dataset.

To perform principal component analysis (PCA), we normalised the data using "SCTransform()" function from *Seurat* package with default settings, then used this as input for the "RunPCA()" function from *Seurat* package. The computed principle components (PCs) were used as input to generate uniform manifold approximation and projection (UMAP) using "RunUMAP()" from *Seurat* package. Unsupervised clustering was performed using "FindNeighbours()" function, followed by "FindClusters()" function from *Seurat* package. Gene signature scoring was performed by computing signature scores for each cell in the dataset using "AddModuleScore()" function from *Seurat* package. Differential gene expression analysis was performed using "FindMarkers()" function from *Seurat* package. Genes with adjusted *P*-values <0.05 were considered as differentially expressed genes.

**Nucleofection**

CRISPR Cas9 gene editing was performed on unstimulated mouse $CD4^+$ T cells. Mouse splenic $CD4^+$ T cells were isolated using an EasySep Mouse $CD4^+$ T cell Enrichment Kit (STEMCELL Technologies), according to the manufacturers' instructions. A 3:1 ratio of Cas9-RNP complex was prepared by mixing 2µl sgRNA (120pmol) (Synthego) and 2µl Cas9 (40pmol) (QB3 Macrolab) followed by incubation at 37°C for 15 minutes. Multi-guides used for each gene were; *Bhlhe40*: A*A*A*CUUACAAACUGCCGCAC, C*G*A*GUGCAUUGCCCAGCUGA, U*C*U*GGGCAGAAGAACUGGGU; *Tcf7*: U*A*A*GAAUCGCGACAGCGCUG, G*C*A*GCUCGUCGGGCGCGCCG, A*U*G*CCGCAGCUGGACUCGGG. Using Amaxa™ P4 primary cell 96-well Nucleofection™ kit (Lonza), 1-5x$10^6$ $CD4^+$ T cells in 20µL P4 buffer was added to the 2µL of RNP mixture, and the total 24µL mixture was transferred to a nucleofection well strip. Nucleofection was performed using the Amaxa™ Nucleofector 96-well shuttle system

764 (Lonza), selecting program DS137. Afterwards, 100µL of 37°C T cell culture media
765 (cRPMI, see *Supplementary 8.1. General reagents*) was added to cell samples and
766 transferred to a 96 U-bottom well plate, followed by addition of 125µL cRPMI. 1µL of
767 2500ng/mL recombinant mouse IL-7 and 2.5µL of 200µg/mL IL-2 was then added to each
768 well and incubated for 48 hours at 37°C in 5% (v/v) CO2. For *in vivo* functional studies, a
769 $1x10^6$ cells/200µL dPBS mix containing equal amounts, confirmed by flow cytometry, of
770 CRISPR/Cas9 gene edited and negative control naïve $CD4^+$ T cells were intravenously
771 injected into B6.$CD45.1^+$ recipient mice via a lateral tail vein.

772 ***In vitro* CD4⁺ T cell polarisation**

773 For *in vitro* polarisation, a 96 flat-well plate was coated with 100µL of 5µg/mL anti-CD3ε
774 mAb (Biolegend). CRISPR/Cas9 gene edited and negative control $CD4^+$ T cells ($2.5x10^5$)
775 supplemented with 5µg/mL anti-CD28 mAb (Biolegend) and 2.5ng/ml recombinant mouse
776 IL-2 were transferred to the anti-CD3ε-coated flat-well plate, and incubated for 72 hours
777 at 37°C in 5% (v/v) CO2 in the presence of polarising antibodies and cytokines in a final
778 volume of in 250µL of cRPMI. For Th1 polarisation: 20ng/mL IL-12 (Biolegend), and
779 20µg/mL αIL-4 mAb (Biolegend); Tr1 polarisation: 20ng/mL IL-12, 200ng/mL IL-27
780 (Prepotech), and 20µg/mL αIL-4 mAb. Cytokine levels from cell culture supernatants were
781 measured by flow cytometry using the Cytometric Bead Array mouse Th1/Th2/Th17
782 Cytokine kit (BD Biosciences) as per manufacturer's instructions on an LSRFortessa™
783 (BD Biosciences), and analysed using FCAP Array™ Software v3.0 (BD Biosciences).

784 **Real-time quantitative PCR**

785 RNA was extracted from $CD4^+$ T cells with the RNeasy Mini Kit (Qiagen) following
786 manufacturer's instructions, RNA was reverse transcribed to cDNA using the ZymoScript
787 RT PreMix Kit (Zymoe) and real-time qPCR was performed with the Gotaq probe Kit
788 (Promega) for mouse *Bhlhe40, Maf* and *Prdm1* on a Bio-Rad CFX 384 real-time PCR
789 system (Bio-Rad) using the TaqMan Gene Expression Assay for *Bhlhe40*
790 (Mm00478592_m1; Applied Biosystems), *Maf* (Mm02581355_s1; Applied Biosystems)
791 and *Prdm1* (Mm00476128_m1 ; Applied Biosystems). Relative expression was
792 normalised relative to mouse *Hprt* (Mm03024075_m1; Applied Biosystems)
793 housekeeping gene.

794 **Cell sorting and adoptive transfer of stem-like and effector PEPCK cells**

795 Spleen mononuclear cells from mice at day 14 of infection with *L. donovani* were stained
796 with CD45.1 FITC (Biolegend), Ly108 APC (Biolegend), CD45.2 PE (Biolegend), CD4
797 BV605 (Biolegend) and CXCR6 BV711 (Biolegend) for 30 minutes at 37°C in the dark
798 followed by SYTOX™ Blue Dead Cell Stain (ThermoFisher Scientific). Cell sorting was
799 performed on a BD FACSAria™ III (BD Biosciences) instrument, with purity confirmed at
800 80-95%. Purified cells were then injected via tail intravenous injection at 1-2.5x$10^5$ cells
801 for Ly108$^-$CXCR6$^+$ PEPCK cells and 6-9x$10^5$ for Ly108$^+$CXCR6$^-$ PEPCK cells.

802 **Statistical analysis**

803 Statistical analyses were performed using Prism 9 (version 9.4.0; GraphPad Software).
804 Statistical testing was performed using either the Mann-Whitney *U*-test or two-ANOVA
805 with Sidak's multiple comparisons test, unless stated otherwise.

806 **Data and materials availability**

807 The materials, data and any associated protocols that support the findings of this study
808 are available from the corresponding author upon request. The raw sequencing data and
809 processed Cell Ranger outputs used in this study will be deposited in an online repository
810 on publication.

811 **Author contributions:**

812 JAE, FDLR, BC, JN, PTB, LB, TCMF and YW generated data, supervised by JAE,
813 FDLR, AH or CRE. JAE, FDLR, BC, SA and HJL analysed data. JAE, AH and CRE
814 conceptualised the study. KC, KHG provided reagents. JAE and CRE led manuscript
815 writing. All authors contributed to and approved the manuscript.

816 **Acknowledgements:**

817 We thank the QIMR Berghofer Flow Cytometry facility, Animal House facility, DNA
818 Sequencing facility, and Genome Informatics Group for their support. We thank the NIH
819 tetramer facility (Atlanta, GA, United States) for production of the I-A$^b$-PEPCK$_{335–351}$
820 tetramer used to detect *L. donovani* PEPCK-specific CD4$^+$ T cells and I-A$^b$-CLIP$_{87-101}$
821 tetramer in these studies. This work was supported by the National Health and Medical

822 Research Council of Australia; Program Grant (1132975) to C.R.E, Senior Research
823 Fellowships to C.R.E (1154265), Australian Infectious Diseases Research Centre
824 University of Queensland-QIMR Berghofer Collaborative Research Scheme to C. R. E.
825 and J. A.E., and QIMR Berghofer Seed Funding Scheme to J.A.E.

826

827

828

829 **References**


830 1. World-Health-Organization. Leishmaniasis. 2023 [cited]Available from:
831 https://www.who.int/news-room/fact-sheets/detail/leishmaniasis

832
833 2. Croft, S.L., Sundar, S. & Fairlamb, A.H. Drug resistance in leishmaniasis. *Clin*
834 *Microbiol Rev* **19**, 111-126 (2006).

835
836 3. Singh, O.P., Hasker, E., Boelaert, M. & Sundar, S. Elimination of visceral
837 leishmaniasis on the Indian subcontinent. *Lancet Infect Dis* **16**, e304-e309
838 (2016).

839
840 4. Singh, O.P., Singh, B., Chakravarty, J. & Sundar, S. Current challenges in
841 treatment options for visceral leishmaniasis in India: a public health perspective.
842 *Infect Dis Poverty* **5**, 19 (2016).

843
844 5. Zijlstra, E.E., Alves, F., Rijal, S., Arana, B. & Alvar, J. Post-kala-azar dermal
845 leishmaniasis in the Indian subcontinent: A threat to the South-East Asia Region
846 Kala-azar Elimination Programme. *PLoS Negl Trop Dis* **11**, e0005877 (2017).

847
848 6. Banchereau, J. *et al.* Immunobiology of dendritic cells. *Annu Rev Immunol* **18**,
849 767-811 (2000).

850
851 7. Engwerda, C.R., Ng, S.S. & Bunn, P.T. The Regulation of CD4(+) T Cell
852 Responses during Protozoan Infections. *Front Immunol* **5**, 498 (2014).

853
854 8. Tubo, N.J. & Jenkins, M.K. CD4+ T Cells: guardians of the phagosome. *Clin*
855 *Microbiol Rev* **27**, 200-213 (2014).

856
857 9. Zhu, J., Yamane, H. & Paul, W.E. Differentiation of effector CD4 T cell
858 populations. *Annu Rev Immunol* **28**, 445-489 (2010).

859
860 10. Tuzlak, S. *et al.* Repositioning T(H) cell polarization from single cytokines to
861 complex help. *Nat Immunol* **22**, 1210-1217 (2021).

862
863 11. Roncarolo, M.G., Gregori, S., Bacchetta, R. & Battaglia, M. Tr1 cells and the
864 counter-regulation of immunity: natural mechanisms and therapeutic applications.
865 *Curr Top Microbiol Immunol* **380**, 39-68 (2014).


866

867 12. Nylen, S. *et al.* Splenic accumulation of IL-10 mRNA in T cells distinct from
868 CD4+CD25+ (Foxp3) regulatory T cells in human visceral leishmaniasis. *J Exp*
869 *Med* **204**, 805-817 (2007).

870
871 13. Edwards, C.L. *et al.* A molecular signature for IL-10-producing Th1 cells in
872 protozoan parasitic diseases. *JCI Insight* **8** (2023).

873
874 14. Edwards, C.L. *et al.* IL-10-producing Th1 cells possess a distinct molecular
875 signature in malaria. *J Clin Invest* **133** (2023).

876
877 15. Montes de Oca, M., Good, M.F., McCarthy, J.S. & Engwerda, C.R. The Impact of
878 Established Immunoregulatory Networks on Vaccine Efficacy and the
879 Development of Immunity to Malaria. *J Immunol* **197**, 4518-4526 (2016).

880
881 16. Montes de Oca, M. *et al.* Blimp-1-Dependent IL-10 Production by Tr1 Cells
882 Regulates TNF-Mediated Tissue Pathology. *PLoS Pathog* **12**, e1005398 (2016).

883
884 17. Engwerda, C.R. & Kaye, P.M. Organ-specific immune responses associated with
885 infectious disease. *Immunol Today* **21**, 73-78 (2000).

886
887 18. Montes de Oca, M., Engwerda, C.R. & Kaye, P.M. Cytokines and splenic
888 remodelling during Leishmania donovani infection. *Cytokine X* **2**, 100036 (2020).

889
890 19. Stanley, A.C. & Engwerda, C.R. Balancing immunity and pathology in visceral
891 leishmaniasis. *Immunol Cell Biol* **85**, 138-147 (2007).

892
893 20. Barazandeh, A.F. *et al.* The Phosphoenolpyruvate Carboxykinase Is a Key
894 Metabolic Enzyme and Critical Virulence Factor of Leishmania major. *J Immunol*
895 **206**, 1013-1026 (2021).

896
897 21. Mou, Z. *et al.* Identification of broadly conserved cross-species protective
898 Leishmania antigen and its responding CD4+ T cells. *Sci Transl Med* **7**, 310ra167
899 (2015).

900
901 22. Southgate, B.A. & Oriedo, B.V. Studies in the epidemiology of East African
902 leishmaniasis. 3. Immunity as a determinant of geographical distribution. *J Trop*
903 *Med Hyg* **70**, 1-4 (1967).

904
905 23. Snook, J.P., Kim, C. & Williams, M.A. TCR signal strength controls the
906 differentiation of CD4(+) effector and memory T cells. *Sci Immunol* **3** (2018).

24. Tubo, N.J. *et al.* Single naive CD4+ T cells from a diverse repertoire produce different effector cell types during infection. *Cell* **153**, 785-796 (2013).

25. Montes de Oca, M. *et al.* IL-27 signalling regulates glycolysis in Th1 cells to limit immunopathology during infection. *PLoS Pathog* **16**, e1008994 (2020).

26. Ng, S.S. *et al.* The NK cell granule protein NKG7 regulates cytotoxic granule exocytosis and inflammation. *Nat Immunol* **21**, 1205-1218 (2020).

27. Kumar, B.V. *et al.* Human Tissue-Resident Memory T Cells Are Defined by Core Transcriptional and Functional Signatures in Lymphoid and Mucosal Sites. *Cell Rep* **20**, 2921-2934 (2017).

28. Mackay, L.K. *et al.* Hobit and Blimp1 instruct a universal transcriptional program of tissue residency in lymphocytes. *Science* **352**, 459-463 (2016).

29. Cook, M.E., Jarjour, N.N., Lin, C.C. & Edelson, B.T. Transcription Factor Bhlhe40 in Immunity and Autoimmunity. *Trends Immunol* **41**, 1023-1036 (2020).

30. Huynh, J.P. *et al.* Bhlhe40 is an essential repressor of IL-10 during Mycobacterium tuberculosis infection. *J Exp Med* **215**, 1823-1838 (2018).

31. Lin, C.C. *et al.* Bhlhe40 controls cytokine production by T cells and is essential for pathogenicity in autoimmune neuroinflammation. *Nat Commun* **5**, 3551 (2014).

32. O'Neal, K.A., Zeltner, S.L., Foscue, C.L. & Stumhofer, J.S. Bhlhe40 limits early IL-10 production from CD4(+) T cells during Plasmodium yoelii 17X infection. *Infect Immun* **91**, e0036723 (2023).

33. Yu, F. *et al.* The transcription factor Bhlhe40 is a switch of inflammatory versus antiinflammatory Th1 cell fate determination. *J Exp Med* **215**, 1813-1821 (2018).

34. Li, C. *et al.* The Transcription Factor Bhlhe40 Programs Mitochondrial Regulation of Resident CD8(+) T Cell Fitness and Functionality. *Immunity* **51**, 491-507 e497 (2019).

35. Gattinoni, L., Speiser, D.E., Lichterfeld, M. & Bonini, C. T memory stem cells in health and disease. *Nat Med* **23**, 18-27 (2017).

947
948 36. Kunzli, M. & Masopust, D. CD4(+) T cell memory. *Nat Immunol* **24**, 903-914
949 (2023).

950
951 37. Zhao, X., Shan, Q. & Xue, H.H. TCF1 in T cell immunity: a broadened frontier.
952 *Nat Rev Immunol* **22**, 147-157 (2022).

953
954 38. Zou, D. *et al.* CD4(+) T cell immunity is dependent on an intrinsic stem-like
955 program. *Nat Immunol* **25**, 66-76 (2024).

956
957 39. Gebhardt, T., Park, S.L. & Parish, I.A. Stem-like exhausted and memory CD8(+)
958 T cells in cancer. *Nat Rev Cancer* **23**, 780-798 (2023).

959
960 40. Tsui, C. *et al.* MYB orchestrates T cell exhaustion and response to checkpoint
961 inhibition. *Nature* **609**, 354-360 (2022).

962
963 41. Schluns, K.S. & Lefrancois, L. Cytokine control of memory T-cell development
964 and survival. *Nat Rev Immunol* **3**, 269-279 (2003).

965
966 42. Faleiro, R.J., Kumar, R., Hafner, L.M. & Engwerda, C.R. Immune regulation
967 during chronic visceral leishmaniasis. *PLoS Negl Trop Dis* **8**, e2914 (2014).

968
969 43. Schnell, A., Littman, D.R. & Kuchroo, V.K. T(H)17 cell heterogeneity and its role
970 in tissue inflammation. *Nat Immunol* **24**, 19-29 (2023).

971
972 44. Song, W. & Craft, J. T Follicular Helper Cell Heterogeneity. *Annu Rev Immunol*
973 **42**, 127-152 (2024).

974
975 45. Murphy, K.M. & Stockinger, B. Effector T cell plasticity: flexibility in the face of
976 changing circumstances. *Nat Immunol* **11**, 674-680 (2010).

977
978 46. O'Shea, J.J. & Paul, W.E. Mechanisms underlying lineage commitment and
979 plasticity of helper CD4+ T cells. *Science* **327**, 1098-1102 (2010).

980
981 47. Becattini, S. *et al.* T cell immunity. Functional heterogeneity of human memory
982 CD4(+) T cell clones primed by pathogens or vaccines. *Science* **347**, 400-406
983 (2015).

984

985 48. Zander, R., Khatun, A., Kasmani, M.Y., Chen, Y. & Cui, W. Delineating the
986 transcriptional landscape and clonal diversity of virus-specific CD4(+) T cells
987 during chronic viral infection. *Elife* **11** (2022).

988
989 49. Engwerda, C. *et al.* A Role for tumor necrosis factor-α in remodeling the splenic
990 marginal zone during *Leishmania donovani* infection. *The American Journal of*
991 *Pathology* **161**, 429-437 (2002).

992
993 50. Mueller, S.N. & Mackay, L.K. Tissue-resident memory T cells: local specialists in
994 immune defence. *Nat Rev Immunol* **16**, 79-89 (2016).

995
996 51. Kamanaka, M. *et al.* Expression of interleukin-10 in intestinal lymphocytes
997 detected by an interleukin-10 reporter knockin tiger mouse. *Immunity* **25**, 941-
998 952 (2006).

999
1000 52. Stetson, D.B. *et al.* Constitutive cytokine mRNAs mark natural killer (NK) and NK
1001 T cells poised for rapid effector function. *J Exp Med* **198**, 1069-1076 (2003).

1002
1003 53. Hao, Y. *et al.* Integrated analysis of multimodal single-cell data. *Cell* **184**, 3573-
1004 3587 e3529 (2021).

1005
1006 54. Im, S.J. *et al.* Defining CD8+ T cells that provide the proliferative burst after PD-1
1007 therapy. *Nature* **537**, 417-421 (2016).

1008

1009

1010

## Extended Data Figures:

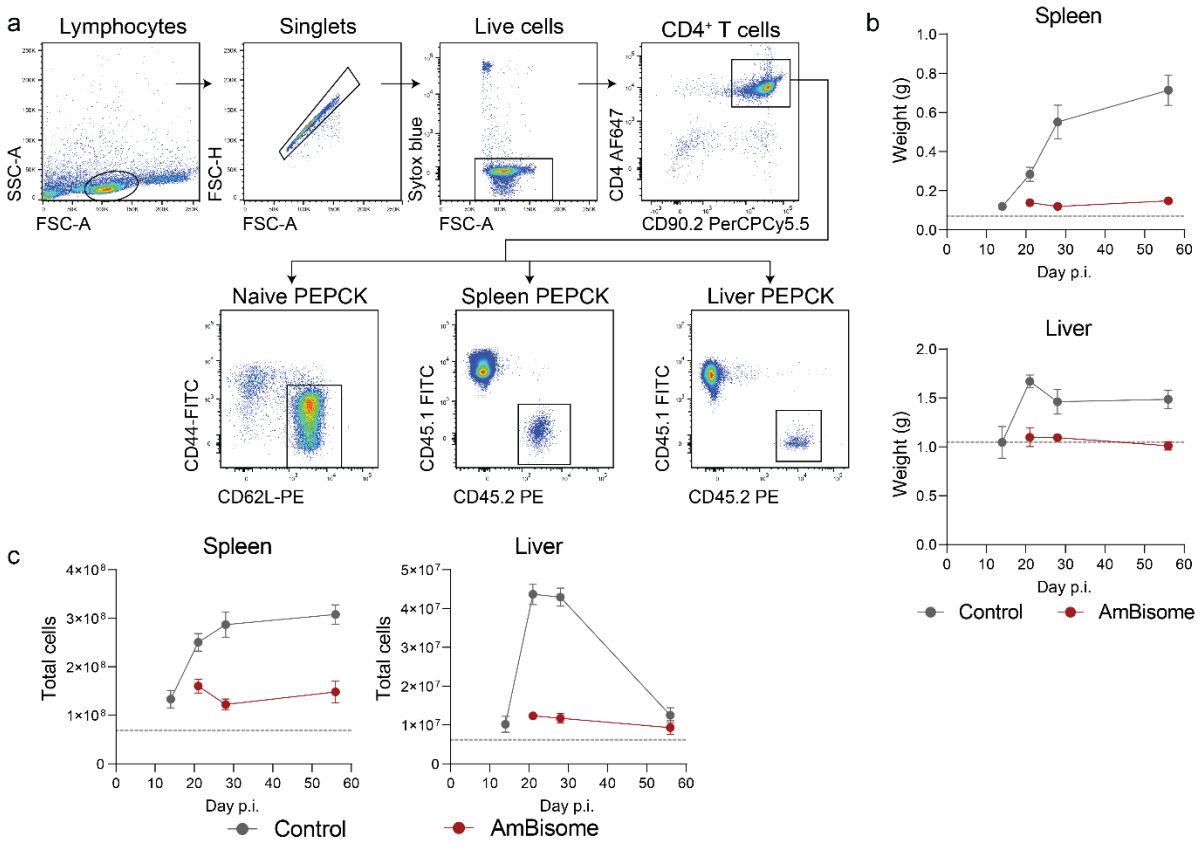


***Extended Data Figure 1*** *(related to Figure 1).* ***(a)*** *Flow cytometry gating strategy for isolating PEPCK cells at day 0 (Naïve PEPCK), or from day 14 p.i. onwards from the spleen and liver (Spleen PEPCK, Liver PEPCK) for scRNAseq assessment.* ***(b)*** *Spleen and liver weights and* ***(c)*** *the total number of cells per spleen and liver of B6.CD45.1⁺ mice infected with L.donovani treated with vehicle control (control) or AmBisome (n = 3-5 mice per group). Error bars represent mean ± SEM.*

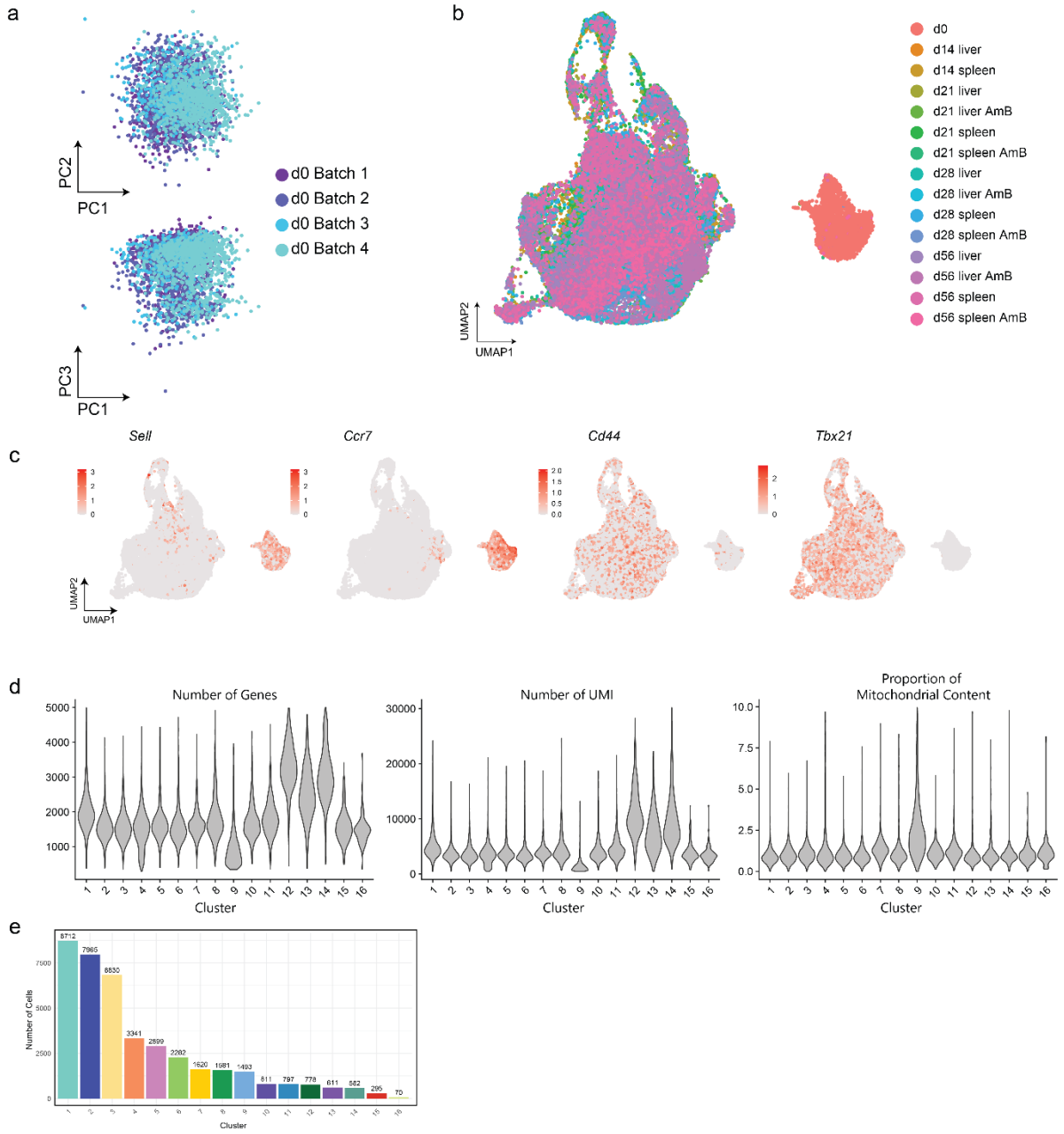


***Extended Data Figure 2*** *(related to Figure 1).* ***(a)*** *Principal component (PC) analysis showing day 0 PEPCK cells from Batch 1-4.* ***(b)*** *UMAP visualisation showing PEPCK cells from day 0-56 p.i. from the spleen and liver from vehicle control and AmBisome- (AmB) treated mice.* ***(c)*** *UMAP visualisation showing the expression of Sell, Ccr7, Cd44 and Tbx21.* ***(d)*** *Distribution of PEPCK cells from day 14-56 p.i. after filtering for number of genes (200<nGenes<5000) and percentage of mitochondrial content (<10%).* ***(e)*** *Bar graph showing the number of cells per cluster.*

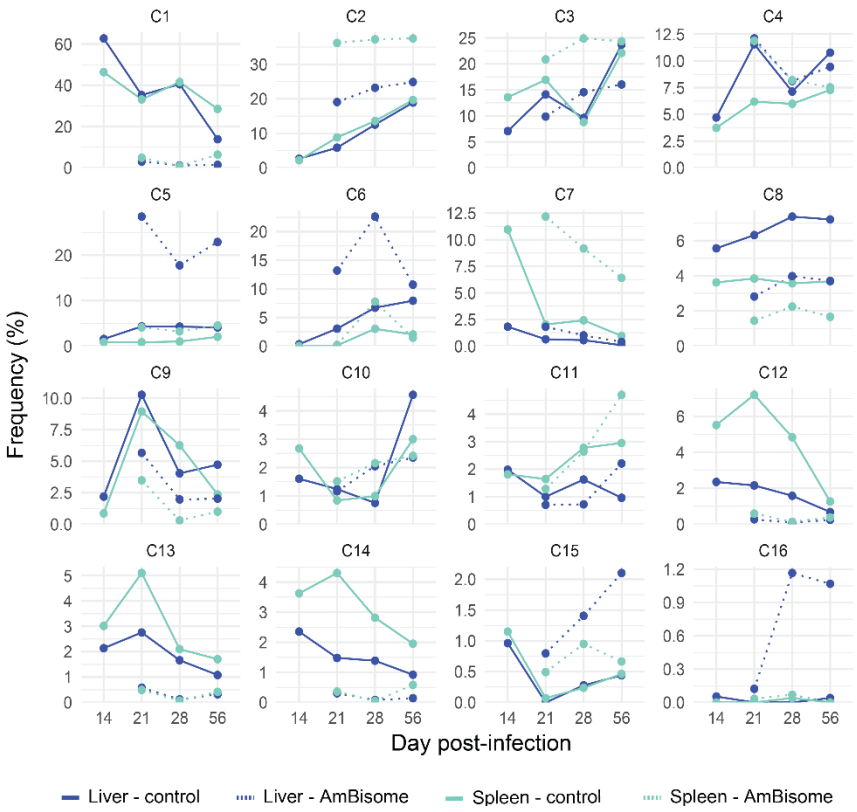


***Extended Data Figure 3*** *(related to Figure 2). Proportion of total cells per sample for each cluster (C1-C16).*

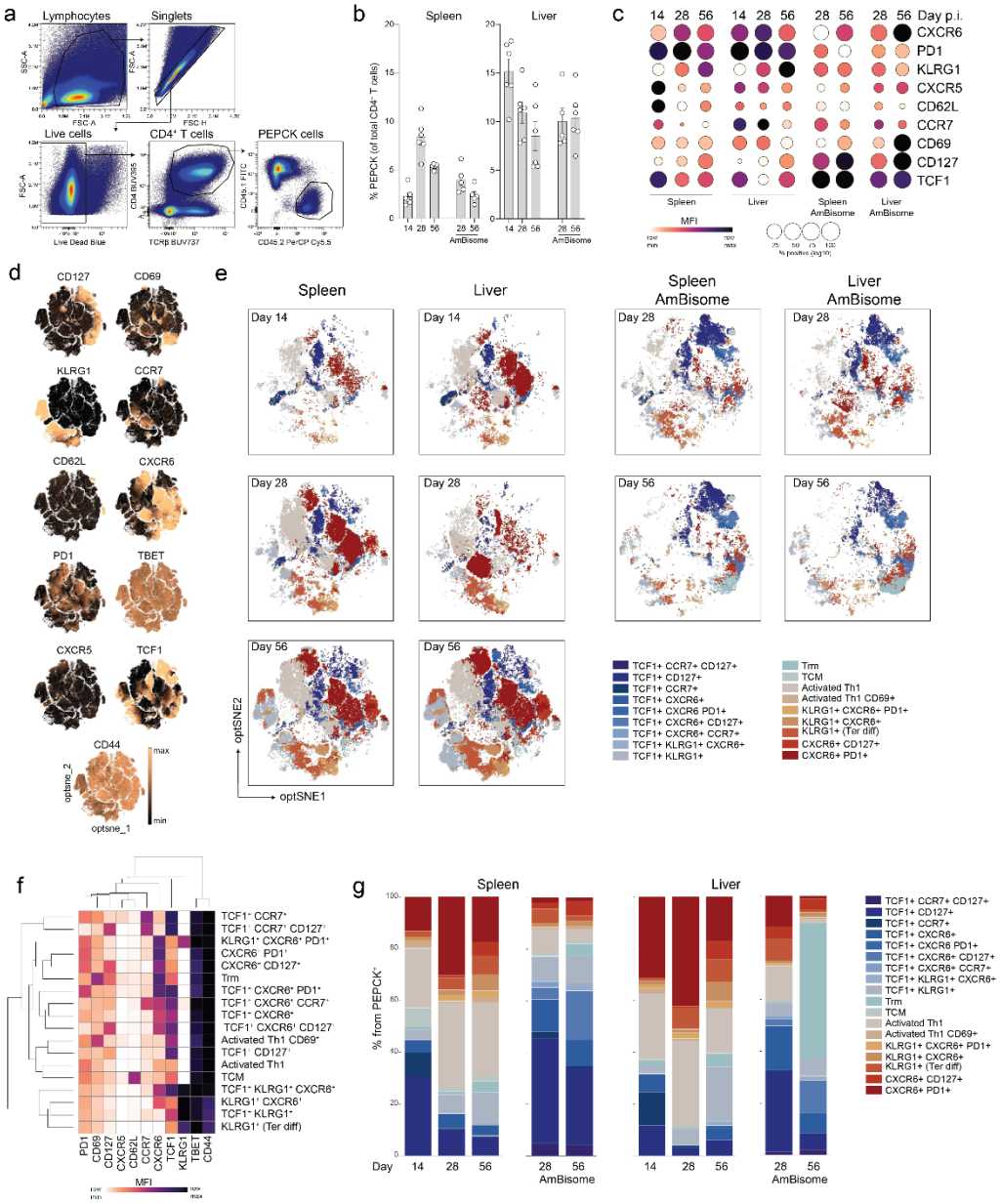


***Extended Data Figure 4*** *(related to Figure 2).* ***(a)*** *Flow cytometry gating strategy to identify PEPCK cells.* ***(b)*** *Graph showing the percentage of PEPCK cells in the spleen and liver from day 14 to 56 p.i.. Data are from one experiment, n = 5/6 mice. Error bars represent mean ± SEM.* ***(c)*** *Dot plot summarizing the average expression (as mean fluorescent intensity; MFI) and percentage (as postitive events) for PEPCK cells from day 14-28 p.i..* ***(d)*** *optSNE plots showing the expression of CD127, CD69, KLRG1, CCR7, CD62L, CXCR6, PD1, TBET, CXCR5, TCF1, and CD44 on PEPCK cells from day 14 – 56 p.i. from the spleen and liver, from mice treated with vehicle control or AmBisome.* ***(e)*** *Clustering of PEPCK cells based on the MFI of all markers shown in (d),* ***(f)*** *and the individual molecule expression for each cluster is shown in the heatmap.* ***(g)*** *Bar graphs showing the distribution of clusters from (e) for each time point and tissue.*

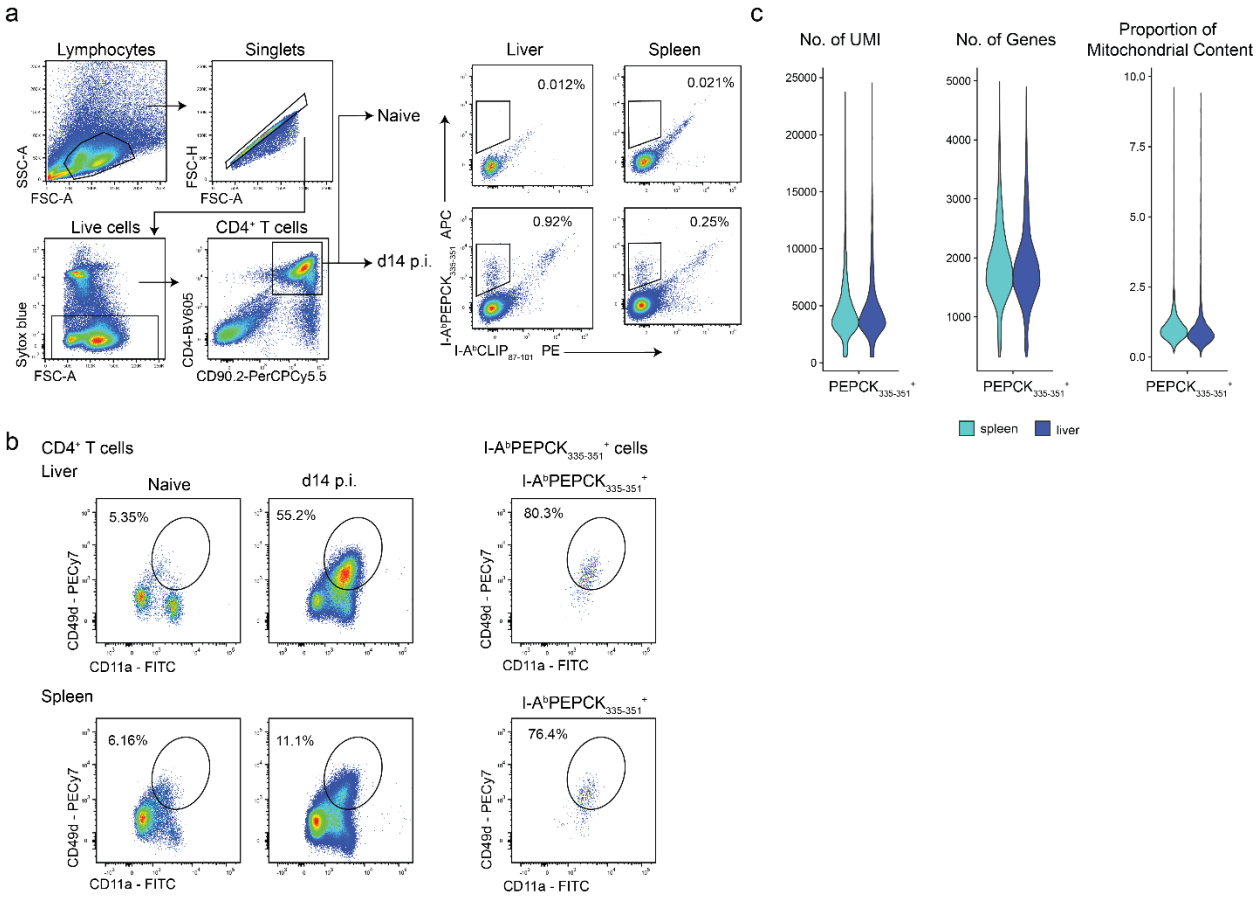


***Extendend Data Figure 5*** *(related to Figure 3).* ***(a)*** *Flow cytometry gating strategy used to isolate I-A$^b$ PEPCK$_{335-351}^+$ cells.* ***(b)*** *Representative flow cytometry plots showing the expression of CD49d and CD11a on CD4+ T cells (left) and I-A$^b$ PEPCK$_{335-351}^+$ cells (right) in the spleen and liver at day 14 p.i. in experimental VL.* ***(c)*** *Violin plots of I-A$^b$ PEPCK$_{335-351}^+$ cells from day 14 p.i. showing quality control metrics.*

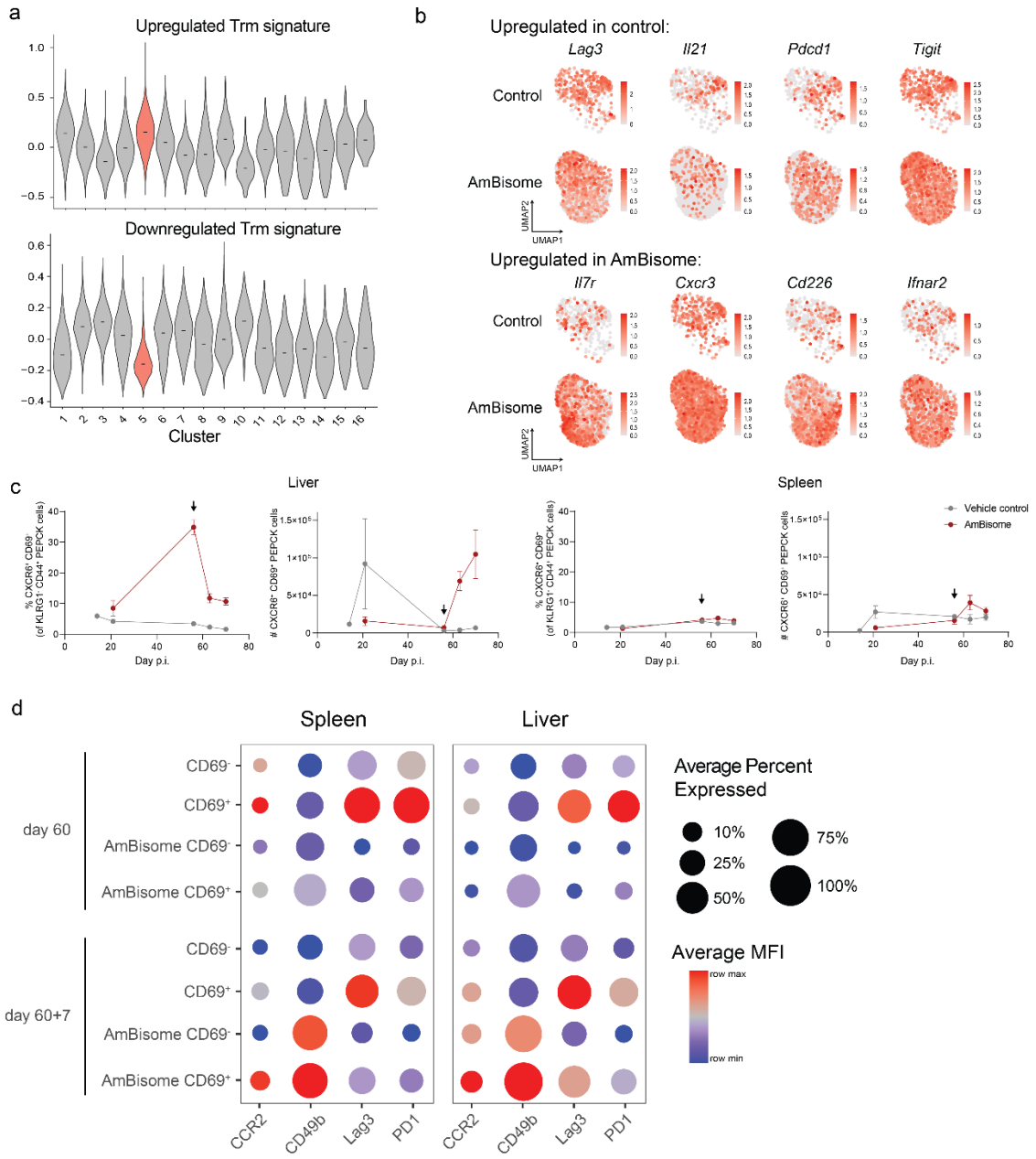


***Extended Data Figure 6*** *(related to Figure 4).* ***(a)*** *Violin plots showing the expression of a Trm gene signature[28], showing genes that are up- or down-regulated across PEPCK cell clusters.* ***(b)*** *UMAP visualisations showing the expression of treatment-associated marker genes in Trm-like PEPCK cells, subsetted by control and AmBisome treatment groups.* ***(c)*** *Graphs showing the percentage and total number of Trm-like PEPCK cells in the spleen and liver during experimental VL,and following rechallenge at day 56 p.i.. Arrows show the day of rechallenge with L. donovani. Data from one experiment, n = 5 mice per group per time point. Error bars show the mean ± SEM* ***(d)*** *Dotplot showing the average expression (as mean fluorescent intensity; MFI) and average percent expressed (as positive events) of CCR2, CD49b, Lag3, and PD1 on PEPCK cells from the spleen and liver at day 60 and seven days post-rechallenge (day 60+7) in experimental VL. Average MFI scaled for each marker.*

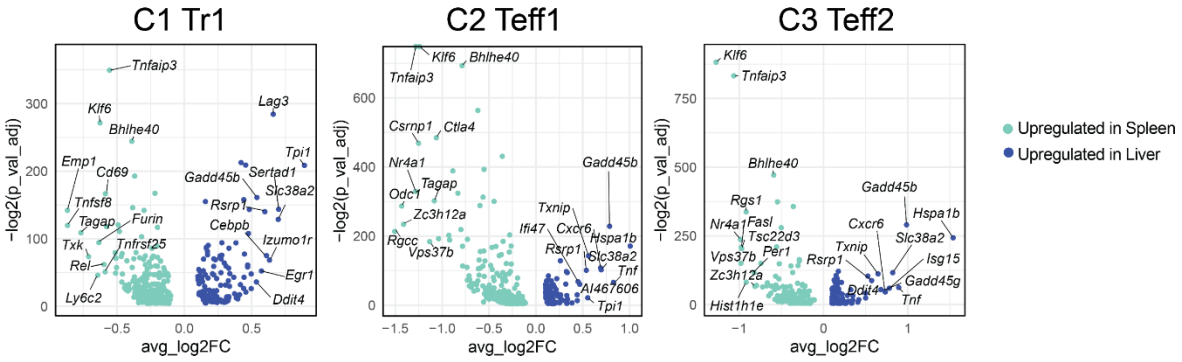


***Extended Data Figure 7*** *(related to Figure 5). Volcano plots showing log2 adjusted P-values and average log2 fold-change for differentially expressed genes between the spleen and liver PEPCK cells for Cluster 1 (C1 Tr1), Cluster 2 (C2 Teff) and Cluster 3 (C3 Teff2). Each cluster was subsetted and differential gene expression analysis was performed between PEPCK cells from the spleen and liver within each cluster using the "FindMarker()" function in Seurat.*

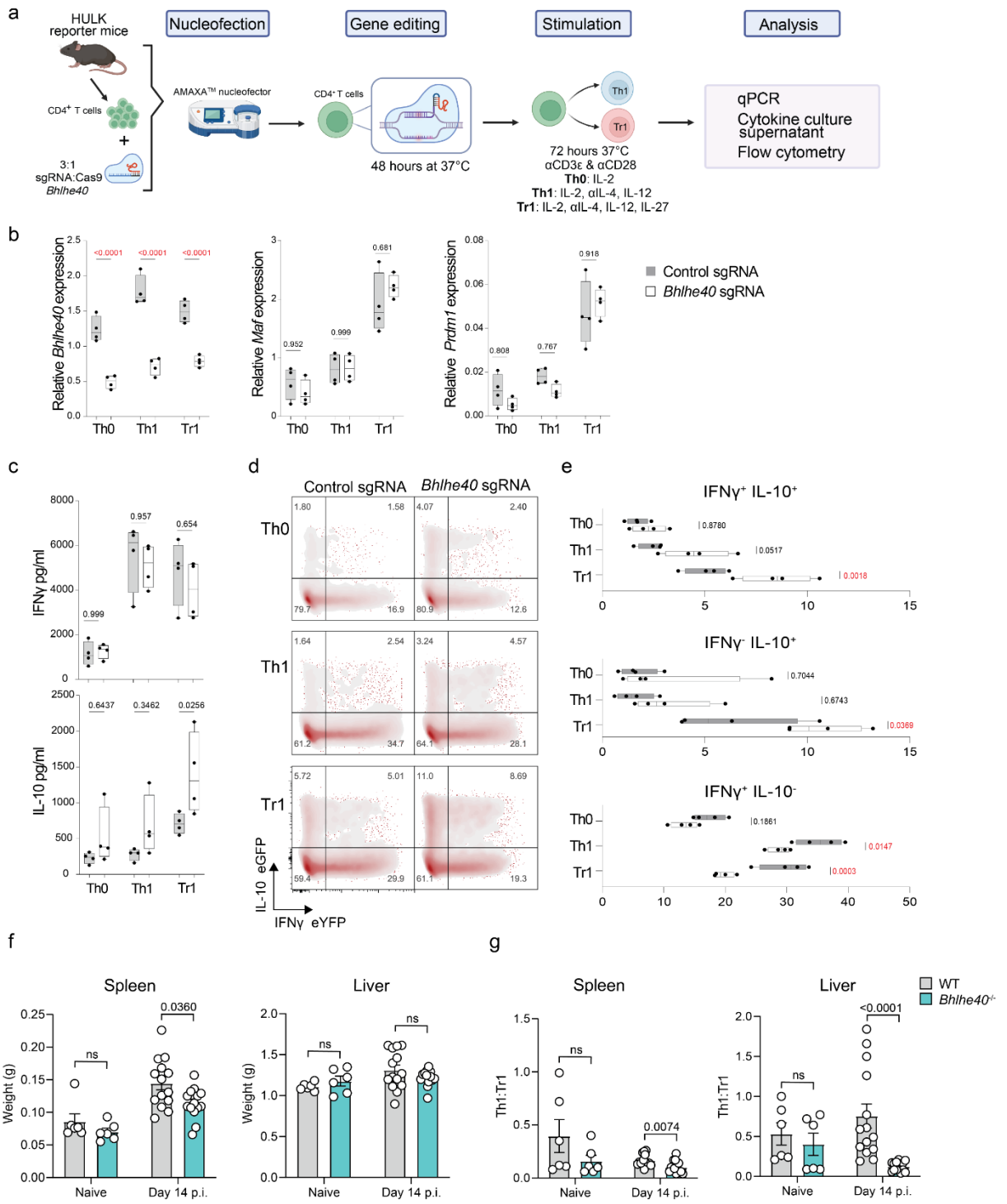


***Extended Data Figure 8*** *(related to Figure 5)*. ***(a)*** *CRISPR/Cas9 editing of Bhlhe40 was performed in primary mouse CD4⁺ T cells from triple reporter (Il10gfp x Ifngyfp x Foxp3rfp) C57BL/6 mice, followed by activation with Th0, Th1, Tr1 conditions and assessment.* ***(b)*** *Bhlhe40, Maf and Prdm1 mRNA expression by CD4⁺ T cells was detected by qPCR and normalised to the housekeeping gene Hprt mRNA. Box plots show the extent of lower and upper quartiles plus*

*median, while whiskers indicate minimum and maximum data points.* ***(c)*** *IFNγ and IL-10 were measured in cell culture supernatants after 72 hours of activation.* ***(d*** *and* ***e)*** *Representative flow cytometry plots and enumeration showing the expression of IFNγ and IL-10 in $CD4^+$ T cells after CRISPR/Cas9 editing and activation. n = 4 mice per condition per experiment. Statistical analysis was performed using two-way ANOVA with Sidak's multiple comparisons test.* ***(f)*** *Spleen and liver weights of wild type (WT) and Bhlhe40$^{-/-}$ mice during L. donovani infection at day 14 p.i..* ***(g)*** *Th1:Tr1 cell ratio determined by flow cytometry. Statistical testing was performed using Mann-Whitney U test. Data are pooled from two experiments, where n = 6 naïve WT and Bhlhe40$^{-/-}$ mice, and n =14 WT and Bhlhe40$^{-/-}$ mice at day 14 p.i..*

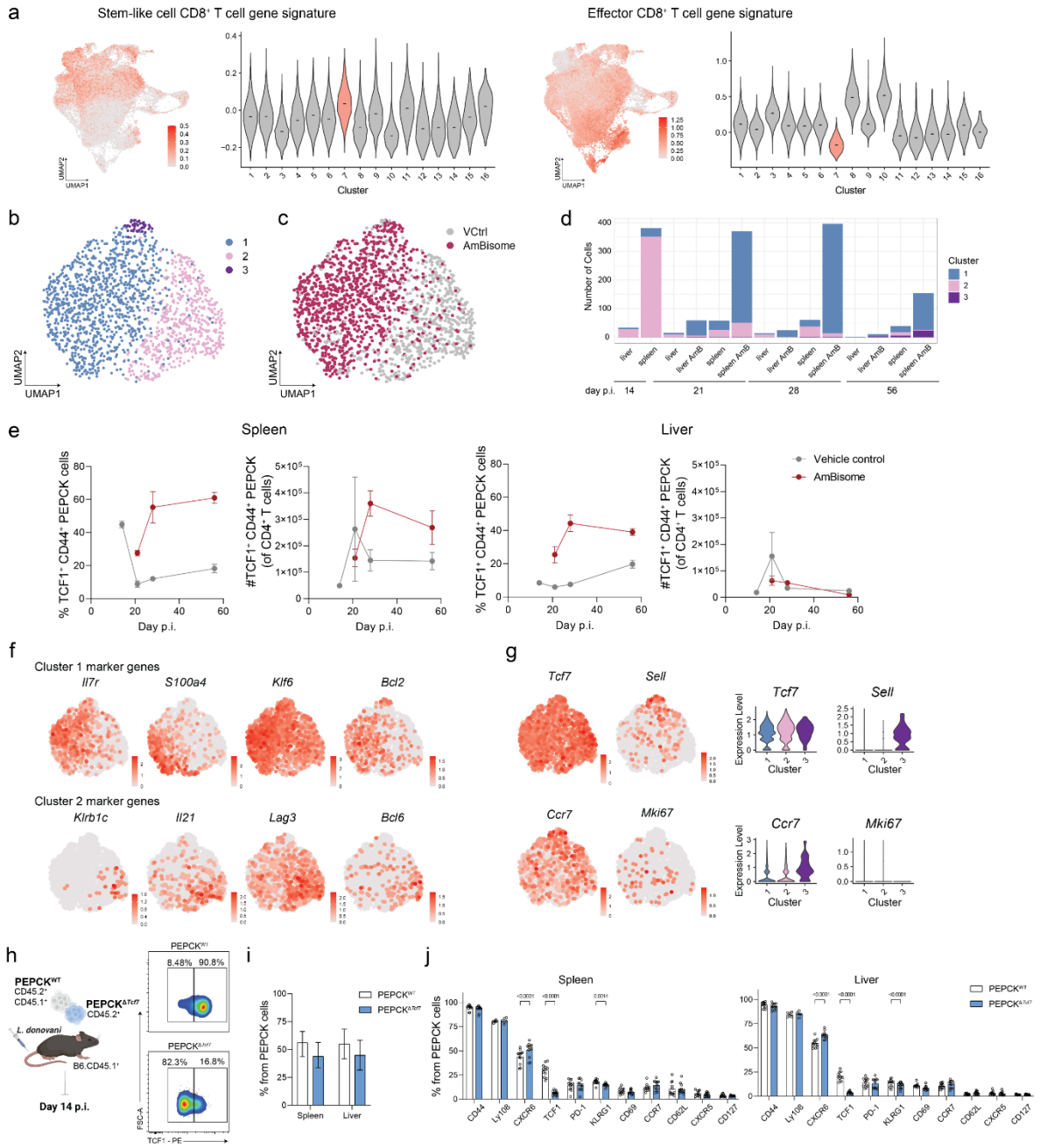


***Extendend Data Figure 9*** *(related to Figure 6).* ***(a)*** *UMAP visualisation and violin plot showing the expression of a stem-like and effector CD8⁺ T cell gene signature[54] on PEPCK cells.* ***(b)*** *UMAP visualisation showing unsupervised clustering of stem-like PEPCK cells and* ***(c)*** *treatment status.* ***(d)*** *Graph showing the number of PEPCK cells in each cluster by sample.* ***(e)*** *Graphs showing the percentage and total number of TCF1⁺CD44⁺ PEPCK cells in the spleen and liver during experimental VL.* ***(f)*** *UMAP visualisations showing the expression of Cluster 1 and 2 marker genes.* ***(g)*** *UMAP visualisations and corresponding violin plots showing the expression of Tcf7, Sell, Ccr7 and Mki67.* ***(h)*** *CRISPR/Cas9 editing of PEPCK cells targeting Tcf7 (PEPCK$^{\Delta Tcf7}$) or a non-specific guide RNA (PEPCK$^{WT}$) was performed and cells were co-transferred into B6.CD45.1⁺ mice, which were then infected with L. donovani. Flow cytometry assessment of PEPCK cells was*

*performed at day 14 p.i.. Flow cytometry plots show the expression of TCF1 on PEPCK$^{WT}$ and PEPCK$^{\Delta Tcf7}$ cells prior to adoptive transfer.* ***(i)*** *Graph showing the frequency of PEPCK$^{WT}$ and PEPCK$^{\Delta Tcf7}$ cells at day 14 p.i. from the spleen and liver.* ***(j)*** *Graphs showing the percentage of surface markers and TCF1 expression on PEPCK$^{WT}$ and PEPCK$^{\Delta Tcf7}$ cells at day 14 p.i. from the spleen and liver. Data are pooled from two independent experiments, with n = 6 mice per group per experiment. Statistical testing was performed using multiple Mann-Whitney U tests.*

**Supplementary Table 1:** Details of antibodies used.

| **Surface:** | | | | | |
|---|---|---|---|---|---|
| **Antibody** | **Fluorophore** | **Clone** | **Company** | **Catalogue #** | **Dilution** |
| CD4 | AF647 | RM4-5 | Biolegend | 100530 | 1:100 |
| CD4 | BUV395 | GK1.5 | BD | 563790 | 1:100 |
| CD4 | BV605 | GK1.5 | Biolegend | 100451 | 1:100 |
| CD90.2 | PerCP Cy5.5 | 53-2.1 | Biolegend | 140322 | 1:100 |
| CD44 | FITC | IM7 | Biolegend | 103022 | 1:100 |
| CD44 | AF700 | IM7 | Biolegend | 103026 | 1:50 |
| CD62L | PE | MEL-14 | Biolegend | 104408 | 1:50 |
| CD62L | BV650 | MEL-14 | Biolegend | 104453 | 1:200 |
| CD45.1 | FITC | A20 | Biolegend | 110706 | 1:50 |
| CD45.1 | PerCP Cy5.5 | A20 | Biolegend | 110728 | 1:50 |
| CD45.2 | PE | 104 | Biolegend | 109808 | 1:50 |
| CD45.2 | PerCP Cy5.5 | 104 | Biolegend | 109826 | 1:50 |
| CD45.2 | Spark Blue 754 | 104 | Biolegend | 285018 | 1:50 |
| CD49d | PE Cy7 | R1-2 | Biolegend | 103618 | 1:100 |
| TCRb | BUV737 | H57-597 | BD | 612821 | 1:200 |
| PD1 | APC-Fire 750 | 29F.1A12 | Biolegend | 135240 | 1:100 |
| KLRG1 | PE-Dazzle 594 | 2F1 | Biolegend | 138424 | 1:200 |
| CCR7 | PE-Cy5 | 4B12 | Biolegend | 120114 | 1:30 |
| CCR5 | PerCP-Cy5.5 | HM-CCR5 | Biolegend | 107016 | 1:50 |
| CD127 | BV421 | A7R34 | Biolegend | 135024 | 1:50 |
| CD69 | BV605 | H1, 2F3 | Biolegend | 104530 | 1:200 |
| CXCR6 | BV711 | J252D4 | Biolegend | 151111 | 1:100 |
| CXCR5 | BV785 | L138D7 | Biolegend | 145523 | 1:50 |
| CD11a | FITC | M17/4 | Biolegend | 101106 | 1:100 |
| Lag3 | BV785 | C9B7W | Biolegend | 125219 | 1:50 |
| CD49b | PE Cy7 | HMα2 | Biolegend | 103518 | 1:50 |
| CCR2 | BV421 | SA203G11 | Biolegend | 150605 | 1:100 |
| Ly108 | APC | 330-AJ | Biolegend | 134610 | 1:100 |
| **Intracellular:** | | | | | |
| **Antibody** | **Fluorophore** | **Clone** | **Company** | **Catalogue #** | **Dilution** |
| TCF1 | PE | C63D9 | Cell Signaling Technologies | 2203S | 1:100 |

| | | | | | |
|---|---|---|---|---|---|
| TCF1 | AF647 | C63D9 | Cell Signaling Technologies | 6709S | 1:100 |
| TBET | PE-Cy7 | 4B10 | Biolegend | 644824 | 1:50 |
| IFNγ | BV650 | XMG1.2 | BD | 563854 | 1:100 |
| IL-10 | PE-Dazzle 594 | JES5-16E3 | Biolegend | 505034 | 1:50 |
| CTLA-4 | BV605 | UC10-4B9 | Biolegend | 106323 | 1:100 |
| Ki67 | APC Fire 750 | 16A8 | Biolegend | 652430 | 1:100 |
| Foxp3 | Ef450 | FJK-16s | eBioscience | 48-5773-82 | 1:100 |
| **scRNAseq hashtagging:** | | | | | |
| TotalSeq™-C0301 anti-mouse Hashtag 1 | - | M1/42 | BioLegend | 155861 | 1:250 |
| TotalSeq™-C0302 anti-mouse Hashtag 2 | - | M1/42 | BioLegend | 155863 | 1:250 |
| TotalSeq™-C0303 anti-mouse Hashtag 3 | - | M1/42 | BioLegend | 155865 | 1:250 |
| TotalSeq™-C0304 anti-mouse Hashtag 4 | - | M1/42 | BioLegend | 155867 | 1:250 |
| TotalSeq™-C0305 anti-mouse Hashtag 5 | - | M1/42 | BioLegend | 155869 | 1:250 |